1 **Correction of frameshift mutations in the *atpB* gene by translational recoding in**

2 **chloroplasts of *Oenothera* and tobacco**

3

4 Irina Malinova[1*], Arkadiusz Zupok[1,2], Amid Massouh[1,3], Mark Aurel Schöttler[1], Etienne H.

5 Meyer[1,4], Liliya Yaneva-Roder[1], Witold Szymanski[1,5], Margit Rößner[1], Stephanie Ruf[1], Ralph

6 Bock[1], Stephan Greiner[1]

7

8 [1] - Department Organelle Biology, Biotechnology and Molecular Ecophysiology, Max Planck

9 Institute of Molecular Plant Physiology, 14476 Potsdam-Golm, Germany

10 [2] – present address: University of Potsdam, Molecular Enzymology, 14476 Potsdam-Golm,

11 Germany

12 3 – present address: Instituto Gulbenkian de Ciência – Fundação Calouste Gulbenkian, Oeiras-

13 Portugal, Rua da Quinta Grande 6, 2780-156 Oeiras, Portugal

14 4 – present address: Institute of Biology/Plant Physiology, Martin-Luther-University Halle-

15 Wittenberg, Weinbergweg 10, 06120 Halle, Germany

16 5 – present address: Max Planck Institute for Terrestrial Microbiology, Core Facility for Mass

17 spectrometry & Proteomics, Karl-von-Frisch-Str. 10, 35043 Marburg, Germany

18

19 *Corresponding author: Irina Malinova (malinova@mpimp-golm.mpg.de)

20

21

22 Short title (≤40 characters): Ribosomal frameshifting in chloroplasts

23

24

25

26

27

28

29 The author responsible for distribution of materials integral to the findings presented in this

30 article in accordance with the policy described in the Instructions for Authors

31 (www.plantcell.org) is: Stephan Greiner (greiner@mpimp-golm.mpg.de).

32 **Abstract**

33 Translational recoding, also known as ribosomal frameshifting, is a process that causes ribosome

34 slippage along the messenger RNA, thereby changing the amino acid sequence of the

35 synthesized protein. Whether the chloroplast employs recoding, is unknown. I-iota, a plastome

36 mutant of *Oenothera* (evening primrose), carries a single adenine insertion in an oligoA stretch

37 of *atpB* (encoding a β-subunit of the ATP synthase). The mutation is expected to cause synthesis

38 of a truncated, non-functional protein. We report that a full-length AtpB protein is detectable in

39 I-iota leaves, suggesting operation of a recoding mechanism. To characterize the phenomenon,

40 transplastomic tobacco lines were generated, in which the *atpB* reading frame was altered by

41 insertions or deletions in the oligoA motif. We found that insertion of two adenines was more

42 efficiently compensated than insertion of a single adenine, or deletion of one or two adenines.

43 We further show that homopolymeric composition of the oligoA stretch is essential for recoding.

44 Plants carrying a disrupted oligoA stretch have an albino-phenotype, indicating absence of indel

45 correction. Our work provides evidence for the operation of translational recoding in

46 chloroplasts. Recoding enables correction of frameshift mutations and can restore

47 photoautotrophic growth in mutants that otherwise would be lethal.

48

Introduction

Plastids (chloroplasts) are plant organelles that harbor their own genome (plastome) and are essential for many metabolic pathways, including photosynthesis and *de novo* synthesis of amino acids, nucleotides and fatty acids (Jarvis and López-Juez, 2013). As a result of endosymbiosis, they have evolved from a photosynthetic cyanobacterium that was engulfed by a eukaryotic cell (Herrmann, 1997; Bock, 2017). During subsequent coevolution of chloroplast and nuclear genomes, many plastid-encoded genes were lost or transferred to the nucleus (Timmis et al., 2004). Therefore, extant plastid genomes are small, and contain only coding information for approximately 120 genes in green plants (Bock, 2007; Barkan, 2011). The majority of these plastid-encoded genes are crucial for plant viability and required for photoautotrophic growth, including, for example, genes encoding the large subunit of RuBisCO, the reaction center subunits of the two photosystems, and subunits of the cytochrome b_6f complex and the adenosine triphosphate (ATP) synthase. Other plastid-encoded gene products comprise components of the chloroplast gene expression machinery, such as the plastid-encoded bacterial-type RNA polymerase (PEP), the ribosomal RNAs (rRNAs), all transfer RNAs (tRNAs) and part of the ribosomal proteins. Due to its cyanobacterial ancestry, the chloroplast gene expression machinery is largely of bacterial type (Peled-Zehavi, 2007; Zoschke and Bock, 2018).

Precise genetic decoding is crucial to ensure the correct amino acid sequence in expressed proteins. During translation, spontaneous frameshifting is very rare with a frequency of about 10^{-4}-10^{-5} per codon (Parker, 1989; Kurland, 1992). However, evidence has accumulated for the non-universality and plasticity of genetic decoding in many systems (Baranov et al., 2015; Atkins et al., 2016). Two major types of alternative genetic decoding can be distinguished: global codon reassignment and local transcriptional and translational recoding (Baranov et al., 2015). Global recoding leads to deviations from the standard genetic code. For example, in some bacteria, the stop codon UGA is reassigned to code for tryptophan (Yamao et al., 1985; McCutcheon et al., 2009) or glycine (Ivanova et al., 2014). Genetic code reassignment was also detected in plastids of the parasitic plant genus *Balanophora*, where UAG is reassigned from a stop codon to tryptophan (Su et al., 2019). At the local level, alternative genetic decoding can be caused by mRNA editing, transcriptional slippage or ribosomal frameshifting (Gesteland et al., 1992).

Transcriptional slippage or RNA polymerase stuttering is a process, by which the nascent transcript or transcriptional complex slips along the DNA template, resulting in the incorporation

80   of additional or fewer nucleotides than encoded by the DNA template (Anikin et al., 2010).

81   Transcriptional slippage mostly affects transcription of longer homopolymeric nucleotide tracts

82   (Baranov et al., 2005), and results in the synthesis of a heterogeneous mRNA population. The

83   slippage can occur during all phases of the transcription cycle (Anikin et al., 2010). RNA

84   polymerase stuttering is frequently seen in some groups of RNA viruses, including

85   paramyxoviruses (Jacques et al., 1994), the Ebola virus (Volchkov et al., 1995), the hepatitis C

86   virus (Ratinier et al., 2008), and plants viruses of the *Potyviridae* family (Olspert et al., 2015).

87   Here it often leads to the synthesis of more than one functional gene product from a single open

88   reading frame (Volchkov et al., 1995; Hausmann et al., 1999). In a few cases, it also has been

89   shown to compensate a frameshift mutation in the coding region (Baranov et al., 2005). For

90   example, a single nucleotide deletion in the human apolipoprotein B (*apoB*) gene causes

91   hypobetalipoproteinemia. However, the mutant allele is not a null allele, because, in addition to

92   the expected truncated protein, some functional full-length ApoB protein was detected (Linton et

93   al., 1992) that presumably was synthesized by transcriptional slippage.

94   Recoding at the level of translation can occur by programmed ribosomal frameshifting

95   (PRF), a process in which the ribosome changes the frame it translates (Ketteler, 2012; Baranov

96   et al., 2015; Atkins et al., 2016). PRF can occur in forward or reverse direction (relative to the 0-

97   frame) as a consequence of the ribosome either skipping one nucleotide (+1) or slipping back

98   one nucleotide (-1) (Ketteler, 2012). This can result in the production of two (or more) proteins

99   from the same mRNA (Caliskan et al., 2017). Various signals are known to affect the efficiency

100 of ribosomal frameshifting such as presence of a Shine-Dalgarno-like sequence upstream of the

101 slip site and the mRNA secondary structure downstream of the slip site (Baranov et al., 2006). -1

102 frameshifting is more common than +1 frameshifting and, therefore, -1 PRFs has been analyzed

103 in more detail (Belew and Dinman, 2015). -1 ribosomal frameshifting requires the slippery

104 sequence motif X_XXY_YYZ, where X denotes any three identical nucleotides, Y denotes A or

105 U, and Z is A, U, or C (Brierley et al., 1992). The P- and A-sites of the tRNA anticodon re-pair

106 from XXY to XXX and YYZ to YYY, respectively (Jacks et al., 1988). In agreement with the

107 consensus sequence, the slip site can be homopolymeric such as the A_AAA_AAA site in the

108 adenomatous polyposis coli (APC) tumor suppressor protein of some nematodes (Baranov et al.,

109 2011). The best-described bacterial -1 frameshift has the type A_AA.A_AA.G (with the codons

110 of the original frame being separated by an underlined space, and the codons in the shifted frame

111   by a dot) (Baranov et al., 2006). A pseudoknot in the mRNA structure is another motif that is

112   often involved in successful ribosomal frameshifting. The pseudoknot consists of two or more

113   stem-loop motifs and resides 3' of the slippery site, separated from it by a spacer region of 5-9 nt

114   (Ketteler, 2012). Together, slippery sequence and RNA secondary structures enable pausing of

115   the ribosome and eventually frameshifting (Namy et al., 2006).

116   While the mechanisms of transcriptional slippage and translational frameshifting are

117   distinct, both can occur on similar sites (Atkins et al., 2016). In *Escherichia coli*, synthesis of

118   functionally distinct DNA polymerase III subunits (τ and γ) is achieved by ribosomal

119   frameshifting, whereas in *Thermus thermophiles*, this is the result of transcriptional slippage

120   followed by standard translation of the multiple mRNAs (Larsen et al., 2000). It is sometimes

121   difficult to distinguish between low levels of transcriptional slippage and ribosomal

122   frameshifting (Atkins et al., 2016). For example, recoding in the core protein of the hepatitis C

123   virus was first ascribed to PRF, but later attributed to transcriptional slippage (Ratinier et al.,

124   2008).

125   Ribosomal frameshifting in plants has been shown to occur on some viral RNAs (Miller

126   and Giedroc, 2010; Atkins et al., 2016). Recently, it was reported that a conserved peptide

127   upstream open reading frame (CPuORF) in the mRNA of *AT3G57170* is a possible candidate for

128   ribosomal frameshifting in *Arabidopsis* (van der Horst et al., 2019). Furthermore, ribosomal

129   frameshifting was detected *in vitro* using wheat-germ extract (Napthine et al., 2003). Finally,

130   indirect evidence for PRF was reported in chloroplasts (Kohl and Bock, 2009). By generating

131   transplastomic tobacco plants, it was shown that the bacterial IS150 transposon was mobilized

132   inside the chloroplast, which results in the accumulation of transposition intermediates. Since the

133   synthesis of IS150 transposase requires PRF (Polard et al., 1991; Vögele et al., 1991), PRF was

134   proposed to exist in plastids.

135   Mutants in the chloroplast genome have been proven as a powerful tool in the analysis of

136   chloroplast gene expression and photosynthesis (Schaffner et al., 1995; Landau et al., 2009;

137   Greiner, 2012). Based on their chlorotic phenotypes, a collection of 51 spontaneous chloroplast

138   mutants was isolated in evening primroses (*Oenothera*) (Kutzelnigg and Stubbe, 1974; Stubbe

139   and Herrmann, 1982). Recently, this collection was systematically characterized by full plastome

140   sequencing (Massouh et al., 2016). Chloroplast mutants affecting all photosynthetic complexes

141   as well as the chloroplast translation machinery were identified. This collection also offers great

142   potential to uncover novel mechanisms of chloroplast gene regulation (Greiner, 2012; Massouh

143   et al., 2016). One of the most striking mutant phenotypes observed in this collection was the

144   mottled phenotype of the I-iota mutant. It displays green spots on white leaves which grow with

145   age, leading to a nearly green phenotype (Figure 1C in Massouh et al. 2016). The underlying

146   mutation is a single adenine insertion (+1A) located within an oligoA stretch in the *atpB* gene,

147   encoding the β-subunit of the plastid ATP synthase (Massouh et al., 2016). The AtpB protein is

148   part of the $\alpha_3\beta_3$ catalytic center harboring the nucleotide binding sites of the enzyme (Hahn et al.,

149   2018). Here, we have analyzed the physiological and biochemical consequences of the +1A

150   mutation in the I-iota mutant. We provide evidence for partial rescue of AtpB synthesis by

151   ribosomal frameshifting. To characterize the recoding mechanism, a set of transplastomic

152   tobacco mutants with mutated frameshift sites were generated and analyzed. Recoding efficiency

153   was further assessed using a luciferase-based reporter system in *E. coli*. We present clear

154   evidence for recoding in the chloroplasts depending on length and composition of the slip site

155   and discuss its functional implications.

156

157   **Results**

158   *Molecular and biochemical characterization of the Oenothera I-iota mutant*

159   I-iota was initially identified as chloroplast mutant displaying a mottled phenotype (Sears and

160   Herrmann, 1985; Massouh et al., 2016). When the mutation is present in the homoplasmic stage,

161   the plants cannot grow photoautotrophically. Therefore, to facilitate growth in soil, plants must

162   be kept as variegated plants that are heteroplasmic and contain green nursery tissue (with wild-

163   type chloroplasts) and pale sectors with mutated chloroplasts (Figure 1A). Taking advantage of

164   biparental chloroplast inheritance in evening primrose, appropriate plants can easily be generated

165   by a simple cross. To this end, a maintainer line with the chloroplast genome of *O. parviflora* is

166   crossed to the I-iota mutant originating from *O. elata* (cf. Massouh et al. 2016; Greiner, 2012)

167   (and Material and Methods). In order to confirm that the mosaic pattern of I-iota was not caused

168   by incomplete vegetative sorting-out of the nursery plastome in the mutated I-iota sectors (Figure

169   1A) (cf. Greiner, 2012), tests for homoplasmy in green and mottled tissue were performed. The

170   tests employed a length polymorphism in the plastid *clpP* gene that results in a larger PCR

171   amplification product in the I-iota plastome of *O. elata* compared to the nursery plastome from

172   *O. parviflora* (Greiner et al., 2008). A single fragment of 312 bp was detected in green parts of

173 the plant, product of 465 bp was identified in mottled areas (Figure 1A,B), thus confirming the

174 homoplasmic state of the I-iota mutation in the mottled leaf sectors. To further characterize the

175 phenotype of the I-iota mutant, homoplasmic I-iota plants were grown under mixotrophic

176 conditions in sterile culture with sugar supplementation. Compared to wild-type plants,

177 homoplasmic I-iota mutants were strongly reduced in growth and displayed a pale or variegated

178 phenotype (Figure 1C). Homoplasmy of the I-iota mutant in sterile culture was verified by PCR

179 using the same marker as described above and confirmed for both the pale and green parts of the

180 leaves (Figure 1B, lanes 3 and 4).

181 Even without the knowledge of the underlying mutation, a defect in the chloroplast ATP

182 synthase was predicted for I-iota. Moreover, the AtpB subunit was correctly identified as

183 targeted by the mutation (Herrmann et al., 1980; Sears and Herrmann, 1985). Indeed, the MS

184 analysis of our work confirmed reduced amounts of AtpA, AtpB and AtpE in I-iota tissue

185 compared to the wild type (Figure 2A). However, in the study of Sears and Herrmann (1985) an

186 unexpected high molecular band was recognized, using their anti-AtpE antibody. In the present

187 western blot analysis, no AtpE was detected in I-iota young leaves, but distinct AtpE bands with

188 the expected size of 14.5 kDa were identified in intermediate and mature leaves (Figure 2B). No

189 unspecific high molecular band was detected in I-iota tissue (Supplemental Figure 1), indicating

190 the absence of an AtpB/AtpE fusion product as suggested by Sears and Herrmann (1985).

191 Recently, a single adenine insertion (+1A) in *atpB* was identified as the only mutation in the I-

192 iota plastome (Massouh et al. 2016). The mutation is located within an oligoA stretch near the 5'

193 end of the gene (Figure 1D). The identified mutation results in a premature stop codon and

194 formation of a truncated protein (41 amino acids long; Figure 1D, Table 1). Confirming the

195 previous report of Sears and Hermann (1985), the full-length AtpB protein was detected in I-iota

196 (+1A) leaf tissue by immunoblot analysis (Figure 2B). Importantly, although the AtpB protein

197 level was lower in I-iota (+1A) leaves than in the wild type (*Oe*-WT), no difference in the

198 mobility of the protein band between the wild type and the I-iota was observed. Mature leaves of

199 I-iota contained higher levels of AtpB than young leaves (Figure 2B), suggesting that functional

200 AtpB accumulates over time. This observation can also explain the age-dependent greening

201 phenotype of I-iota mutant plants (Massouh et al., 2016). Analysis of plastid ultrastructure by

202 transmission electron microscopy confirmed the age-dependent developmental gradient in

203 thylakoid membrane formation of I-iota (Figure 2D-F). Although mature leaves of I-iota still

204 have slightly disorganized thylakoid membranes, they are rather similar to wild-type thylakoids
205 (Figure 2C,F).

206   Presence of a full-length AtpB protein in I-iota tissue was verified by in-gel tryptic
207 digestion followed by mass spectrometry (LC-MS/MS; Table 2). Finally, as *in vivo* measure of
208 chloroplast ATP synthase activity, the proton conductivity of the thylakoid membrane (gH^+) was
209 assessed by decay kinetics of the electrochromic shift signal during a short interval of darkness.
210 In mature leaves of I-iota, a residual ATP synthase activity of 29% compared to the wild type
211 was detectable (Figure 3A), confirming that the chloroplast ATP synthase is indeed active in the
212 I-iota mutant. As a consequence of the reduced ATP synthase activity, the entire photosynthetic
213 apparatus of I-iota was affected. The chlorophyll content per leaf area was strongly reduced to
214 24% of the wild-type level, and also the chlorophyll *a/b* ratio was strongly decreased, indicating
215 a substantial loss of photosystems (whose reaction centers exclusively bind chlorophyll *a*), while
216 the antenna proteins (binding both chlorophyll *a* and *b*) were less severely affected (Table 3).
217 Also, F_V/F_M, the maximum quantum efficiency of photosystem II (PSII) in the dark-adapted
218 state, was clearly reduced in I-iota, pointing to PSII photoinhibition and the presence of
219 uncoupled antenna proteins. Finally, light response curves of chlorophyll-*a* fluorescence
220 parameters revealed that linear electron transport (calculated from PSII yield measurements) was
221 strongly decreased in I-iota, and the acceptor side of PSII (here shown as the chlorophyll-*a*
222 fluorescence parameter qL) became more rapidly reduced (Figure 3B). All these changes bear
223 close similarity to photosynthetic defects previously reported for tobacco and mays (*Zea mays*)
224 mutants with strongly diminished accumulation of ATP synthase (Rott et al., 2011; Zoschke et
225 al., 2012), and can be ascribed to an increased proton motive force across the thylakoid
226 membrane (because its consumption by ATP synthase is massively slowed down). This
227 increased proton motive force leads to a strong acidification of the thylakoid lumen, which in
228 turn slows down linear electron transport due to "photosynthetic control" of plastoquinol re-
229 oxidation at the cytochrome b_6f complex (Nishio and Whitmarsh, 1993), and also results in the
230 stronger reduction of the PSII acceptor side, increased photoinhibition of PSII, and loss of
231 photosystems (Rott et al., 2011; Schöttler et al., 2015). Taken together, these data strongly
232 suggest partial compensation of the I-iota (+1A) mutation by a recoding mechanism that operates
233 in I-iota tissue. Interestingly, analysis of the predicted structure of the *atpB* mRNA revealed
234 presence of a potential slip site (oligoA stretch) and a stem-loop-type secondary structure

235 downstream of the slip site (Figure 3C). Both motifs are known to be crucial elements for PRF.

236 In contrast, a homopolymeric nucleotide sequence alone can be sufficient for induction of

237 transcriptional slippage (see Introduction).

238 Independent of the underlying molecular mechanism, mutation compensation is only

239 partial and, therefore, will result in the formation of both in-frame and out-of-frame polypeptides

240 (see Introduction). To characterize the process of mutation correction in I-iota at the protein

241 level, we analyzed the lysine stretch encoded by the oligoA tract in which the mutation is located

242 (Figure 1D). Since frame correction can occur in forward or reverse direction, different scenarios

243 are possible (Table 1): (i) uncorrected gene expression will result in formation of a truncated

244 polypeptide; (ii) +1 correction would lead to the synthesis of a protein identical to the wild type,

245 and (iii) +4 or -2 correction would result in the synthesis of proteins that differ from the wild

246 type in the number of lysines in the stretch (four or two lysines, respectively, instead of three in

247 the wild-type protein). Consequently, resolving the number of lysines and the amino acid

248 sequence downstream is crucial to the understanding of the correction mechanism.

249 Unfortunately, standard trypsin digestion cannot be applied for mass spectrometric peptide

250 identification, because trypsin cleaves at the carboxyl site of lysine and arginine residues

251 (Tsiatsiani and Heck, 2015), and thus, is unsuitable to resolve the number of lysines in a peptide.

252 As an alternative, we used in-gel digestion with glutamyl peptidase I (Glu-C) that cleaves the

253 amino acid chain at aspartate and glutamate residues (Tsiatsiani and Heck, 2015). The peptide

254 sequence information obtained from tandem mass spectrometry (MS/MS) was then analyzed

255 against the *in silico* digested AtpB sequence from wild-type *Oenothera* and possible out-of-

256 frame peptides that could be produced in the I-iota mutant (Table 1, Supplemental Table 1). No

257 in-frame peptides corresponding to the expected truncated polypeptide were detected in I-iota

258 samples, possibly suggesting that the truncated protein is unstable and condemned to rapid

259 degradation. Instead, the same number of three lysines was detected in both the wild type and I-

260 iota, revealing that the I-iota mutant indeed produces the wild-type AtpB proein and strongly

261 suggesting that a +1 correction mechanism operates in the mutant chloroplasts (Figure 3D, Table

262 1).

263

264 ***Reproduction of the I-iota mutation in transplastomic tobacco plants***

265   Comparison of the plastid *atpB* sequences revealed that the oligoA stretch near the 5' end of the

266   coding region is conserved among higher plants and is also present in the cigarette tobacco

267   (*Nicotiana tabacum*; Figure 4A). Moreover, a similar stem-loop structure was predicted to reside

268   downstream of the oligoA tract in the *atpB* mRNAs of *Oenothera* and tobacco (Figure 3C, 4B,).

269   We, therefore, attempted to reproduce the frame-correcting mechanism in tobacco chloroplasts,

270   an experimental system amenable to an easy genetic manipulation. To obtain insights into the

271   sequence requirements for reading frame correction, a set of transplastomic tobacco lines was

272   generated (Figure 5A). To mimic the *Oenothera* I-iota mutation, a single adenine was inserted

273   into the oligoA stretch within the 5' part of the cloned tobacco *atpB* genes, generating plastid

274   transformation vector pIM12 (+1A). The corresponding transplastomic lines will subsequently

275   be referred to as *Nt*-IM12 (+1A) plants. To analyze the role of the oligoA sequence in the

276   induction of recoding, a construct pIM13 (AAG+1A) was generated, in which the oligoA stretch

277   was disrupted by replacing adenines with guanines in the third codon position (Figure 5A).

278   These mutations do not alter the identity of the encoded amino acids, because both AAA and

279   AAG triplets encode lysine. A similar construct with a disrupted oligoA stretch but without the

280   frameshift mutation was generated as control [pIM11 (AAG); Figure 5A]. All transplastomic

281   mutants were produced by biolistic chloroplast transformation using the *aadA* cassette as

282   selectable marker that confers resistance to spectinomycin (Svab and Maliga, 1993; Figure 6A).

283   Insertion of the *aadA* cassette alone did not affect plant growth and chloroplast ATP synthase

284   activity (*aadA-atpB* control plants; Figure 5B; Rott et al., 2011).

285   Replacement of three adenines with guanines in third codon position resulted in a wild-

286   type-like phenotype [*Nt*-IM11 (AAG±0; Figure 5B], as expected. By contrast, *Nt*-IM12 (+1A)

287   plants carrying the same mutation as I-iota (+1A) resembled the mottled phenotype of the

288   *Oenothera* mutant (Figures 1A,C and 5B). Similar to *Oenothera* I-iota plants, transplastomic *Nt*-

289   IM12 (+1A) plants were unable to grow autotrophically. Interestingly, combined disruption of

290   the oligoA stretch and insertion of the I-iota mutation led to an albino phenotype. Transplastomic

291   *Nt*-IM13 (AAG+1) plants are white and resemble the albino phenotypes of transplastomic *ΔatpB*

292   knock-out mutants (Hager, 2002) and other loss-of-function mutants of the chloroplast ATP

293   synthase (Karcher and Bock, 2002; Schmitz-Linneweber et al., 2005). This observation indicates

294   that the oligoA stretch is of crucial importance for the frame-correcting mechanism.

295   Next, we analyzed photosynthesis in the transplastomic tobacco plants to assess their
296   physiological similarity to the *Oenothera* I-iota mutant. No significant differences in linear
297   electron flux and the redox state of the PSII acceptor side (qL) were detected between the wild
298   type (*Nt*-WT), the *aadA-atpB* and the *Nt*-IM11 lines (Figure 5C). Interestingly, although
299   chlorophyll content was similar in *Nt*-IM12 (+1A; the I-iota mutation) and the control lines
300   (Table 3), all other parameters were reduced in *Nt*-IM12 (+1A). Linear electron flux was strongly
301   decreased in *Nt*-IM12 (+1A), and the PSII acceptor side became reduced already in very low
302   actinic light intensities (Figure 5C), similar to the *Oenothera* I-iota mutant. Also, F_V/F_M was
303   strongly reduced in *Nt*-IM12 (+1A), again pointing to PSII photoinhibition and the presence of
304   uncoupled antenna proteins. This conclusion is further supported by the strongly decreased
305   chlorophyll *a/b* ratio of *Nt*-IM12 (+1A), arguing for a predominant loss of the photosystems
306   (Table 3). No analysis of photosynthetic performance was possible for *Nt*-IM13 (AAG+1), since
307   the plants were completely white. In addition, activity of the ATP synthase was determined. As
308   expected, no significant differences in ATP synthase activity between the wild type, the *aadA-*
309   *atpB* control plants and *Nt*-IM11 (AAG) plants were detected (Figure 5D). By contrast, the line
310   *Nt*-IM12 (+1A) displayed a strongly reduced activity of ATP synthase.

311   The observed phenotypes of the transplastomic tobacco lines suggested a varying degree
312   of AtpB correction in the different lines. To explore the correlation between phenotype of the
313   plants and synthesis of full-length AtpB protein, the accumulation of AtpB protein was analyzed
314   by tryptic in-gel digestion followed by LC-MS/MS analysis. Full-length AtpB was detected in
315   the wild type (*Nt*-WT), the control line *aadA-atpB*, and the *Nt*-IM11 (AAG)] and *Nt*-IM12 (+1A)
316   mutants. No AtpB was detected in the white *Nt*-IM13 (AAG+1A) line (Table 2).

317   To compare the mechanism of reading frame correction with the I-iota mutant, the protein
318   bands corresponding to AtpB were subjected to Glu-C digestion and analyzed by LC/MS-MS.
319   As in I-iota, we identified identical peptides covering the slippery site in *Nt*-IM12 (+1A) and
320   wild-type tissue (Figure 5E), suggesting operation of +1 correction also in the chloroplasts of
321   tobacco (Table 1). No peptides derived from other reading frames could be detected (Table 1,
322   Supplemental Table 1).

323

324   ***Influence of mutations in the oligoA stretch on frameshift efficiency in E. coli***

325   The phenotype of the *Oenothera* I-iota mutant and the transplastomic tobacco *Nt*-IM12 (+1A)

326   line strongly suggests the presence of +1 frame correction in the chloroplasts of higher plants.

327   Chloroplasts are of prokaryotic origin (Bock and Timmis, 2008) and have a bacterial-like

328   translation machinery (Zoschke and Bock, 2018). Moreover, structure and subunit composition

329   of CF_1F_0 resembles the ATP synthases of bacteria (Hahn et al., 2018). To test the possibility that

330   the *atpB* reading frame correction also occurs in bacteria and, if it does, precisely measure its

331   efficiency, a dual-luciferase reporter system in *E. coli* was employed (Kramer and Farabaugh,

332   2007). The dual-luciferase reporter assay is a powerful tool to analyze frameshifting efficiencies

333   in various organisms and systems (Grentzmann et al., 1998; Kramer and Farabaugh, 2007;

334   Ketteler, 2012). The assay is based on the Renilla luciferase serving as expression control,

335   whereas the activity of the firefly luciferase depends on the expression of the test sequence

336   (Grentzmann et al., 1998; Kramer and Farabaugh, 2007). Thus, the activity of the firefly

337   luciferase relative to the Renilla luciferase reflects the translation efficiency (Grentzmann et al.,

338   1998).

339   To determine the translation efficiency of our various *atpB* sequences, 150 nt of the 5'

340   part of the *atpB* gene from *Oenothera* and tobacco were cloned into the pEK4 plasmid (Kramer

341   and Farabaugh, 2007) between the Renilla and firefly luciferase genes. In addition, several

342   constructs varying in the length of the oligoA stretch or harboring a disrupted oligoA stretch (by

343   placing guanines into the third codon position; see above) were generated (Supplemental Table

344   2). The translation efficiency measured in the constructs containing the *Oenothera* or tobacco

345   wild-type sequence (pEK4-*Nt*-WT and pEK4-*Oe*-WT) was set as 100%. The pEK4-Nt-IM11

346   (AAG) construct, where the oligoA track of the tobacco WT sequence is destroyed by guanines,

347   displayed an even enhanced efficiency compared to the wild-type sequences (Figure 7). By

348   contrast, single adenine insertions caused a decrease in firefly luciferase activity relative to

349   Renilla luciferase in *Oenothera* and the analogous tobacco constructs [pEK4-*Oe*-WT vs. pEK4-I-

350   iota (+1) and pEK4-*Nt*-WT vs. pEK4-*Nt*-IM12 (+1A); Figure 7]. Similar to the *in planta*

351   situation, disruption of the oligoA stretch in the single adenine insertion construct resulted in a

352   significant reduction of the frameshift efficiency [pEK4-*Nt*-IM12 (+1A) vs. pEK4-*Nt*-IM13

353   (AAG+1A)]. Interestingly, +2A insertion in the oligoA stretch [pEK4-*Nt*-IM14 (+2A)] improved

354   the translation efficiency by ca. 40%. Single or double adenine deletions [pEK4-*Nt*-IM16 (-1A)

355   and pEK4-*Nt*-IM18 (-2A), respectively] did not exhibit effective frame correction and showed

356 only approximately 5% of residual activity (Figure 7). In conclusion, also in the *E. coli*-based

357 assay system, frame correction was detected in all constructs containing the single adenine

358 insertion. Surprisingly, an even higher translation efficiency was detected with the construct with

359 two adenines inserted.

360

361 *Transplastomic tobacco plants with varying lengths of the oligoA stretch*

362 The effective frame correction observed with the pEK4-*Nt*-IM14 (+2A) construct (Figure 7)

363 raised the question how a +2A insertion into the oligoA stretch of *atpB* would affect the plant

364 phenotype. To address this question, additional transplastomic tobacco lines were designed. Line

365 *Nt*-IM14 (+2A) carries a +2A mutation, while lines *Nt*-IM16 (-1A) and *Nt*-IM18 (-2A) carry

366 deletions of one or two adenines, respectively (Figure 8A). Homoplasmy of the generated

367 transplastomic mutants was tested by restriction fragment length polymorphism analysis (Figure

368 6B), and presence of the mutations was verified by Sanger sequencing. Interestingly, *Nt*-IM14

369 (+2A) plants were indistinguishable from the wild type under mixotrophic conditions (Figure

370 8B). Moreover, although clearly retarded in growth, they were even able to grow

371 photoautotrophically (Figure 9A). Compared to the wild type, *Nt*-IM14 (+2A) plants flowered 5-

372 8 months later, but produced viable seeds that could be used for seed tests for homoplasmy

373 (Figure 6C; cf. Material and Methods). Therefore, for *Nt*-IM14 (+2A) and the control lines *aadA-*

374 *atpB* and *Nt*-IM11 (AAG) the full set of physiological parameters could be determined under

375 both mixotrophic and autotrophic conditions (Figure 8C and 9C). Interestingly, plants with a

376 single adenine deletion [*Nt*-IM16 (-1A)] displayed a similar phenotype as plants with a single

377 adenine insertion [*Nt*-IM16 (-1A) vs. *Nt*-IM12 (+1A), Figure 8B vs. Figure 5B]. Both mutants

378 exhibited pale green leaves with white areas. By contrast, the *Nt*-IM18 (-2A) line with the 2A

379 deletion did not resemble the *Nt*-IM14 (+2A) phenotype. *Nt*-IM18 (-2A) plants were white with

380 small green spots (Figure 8B), suggesting that the double adenine deletion cannot be efficiently

381 compensated by recoding. Similar to *Nt*-IM13 (AAG+1), homoplasmic seeds could be obtained

382 from stable periclinal chimeras (cf. Material and Methods). Seedlings that germinated in the

383 presence or absence of spectinomycin were white with occasional green spots (Figure 6C). The

384 visually observed phenotypes were further confirmed by the analysis of photosynthetic

385 parameters: Nt-IM14 (+2) plants displayed a higher chlorophyll content compared to the other

386 plant lines (Table 3), and the photosynthetic parameters of *Nt*-IM12 (+1A) and *Nt*-IM16 (-1A)

387   were similar (Table 3, Figure 8C vs. 5C), suggesting comparable *atpB* correction efficiency. *Nt*-

388   IM14 (+2A) displayed intermediate photosynthetic behavior when compared to WT and +1A or -

389   1A plants (Figures 8C and 9C; Table 3).

390   Next, ATP synthase activity was assessed in the new set of transplastomic lines. The

391   green *Nt*-IM14 (+2A) line displayed the highest ATP synthase activity among all mutants

392   containing frameshift mutations (Figures 8D and 5D). In fact, when compared under mixotrophic

393   and autotrophic growth conditions, *Nt*-IM14 (+2A) plants showed similar ATP synthase activity

394   (19% and 17%, respectively; Figures 8D and 9B). By contrast, ATP synthase activity in *Nt*-IM16

395   (-1A) was at the detection limit, close to the decay kinetics of thylakoids with inactive ATP

396   synthase. The electrochromic shift signal was not measurable in white *Nt*-IM18 (-2A) plants.

397   Finally, proteomic analysis of the transplastomic mutants was performed by tryptic in-gel

398   digestion followed by LC-MS/MS. The AtpB protein was detected in all newly generated lines

399   (Table 2). Peptides derived from the mutated site were generated by Glu-C digestion to gain

400   insight into the correction mechanisms operating (Table 1). Peptides clarifying the amino acid

401   sequence specified by the *atpB* mutations introduced into the transplastomic lines were identified

402   in *Nt*-IM16 (-1A) and *Nt*-IM14 (+2A) (Figure 8E,F). Interestingly, both +2 and -1 corrections

403   were detected in the Nt-IM14 (+2A) line, as evidenced by identification of peptides with two or

404   three lysines (Figure 8F). A peptide resulting from +2 correction was detected in *Nt*-IM16 (-1A)

405   (Figure 5E). No peptides were detected in the white line *Nt*-IM18 (-2A).

406

407   *Analysis of the atpB cDNA in Oenothera and transplastomic tobacco plants*

408   Since RNA polymerase stuttering and ribosomal frameshifting can both occur at homopolymeric

409   sequence motifs, it can be challenging to unambiguously distinguish between the two recoding

410   mechanisms (Atkins et al., 2016). Transcriptional slippage generates a heterogeneous population

411   of mRNAs that can be detected by cDNA analysis. Although seemingly straightforward, the high

412   error rate exhibited by reverse transcriptases can complicate this approach (Roberts et al., 1988).

413   To minimize this problem, we used a high-fidelity reverse transcriptase (a variant of Moloney

414   murine leukemia virus reverse transcriptase, MMLV-RT, that was combined with a 3'-5'

415   exonuclease domain for proofreading). The enzyme exhibits an error rate that is three times

416   lower than that of conventional reverse transcriptases (Arezi and Hogrefe, 2007). cDNA

417   sequence analyses revealed that, in all transplastomic lines, the mutations introduced into the

418   *atpB* locus were faithfully represented in the mature *atpB* mRNAs (Figure 10A). No sequence

419   shifts or double peaks were detected in any of the chromatograms. A similar situation was

420   observed for I-iota and the corresponding *Oenothera* wild type, although an overall somewhat

421   more noisy sequence was obtained here for both the wild-type and the mutant (Figure 10B). To

422   estimate the accuracy of cDNA synthesis and the sensitivity of the assay, we mimicked RNA

423   polymerase stuttering by mixing total RNA from *Nt*-WT and *Nt*-IM14 (+2A) in different ratios

424   followed by reverse transcription and sequence analysis of the amplified cDNA population

425   (Figure 10C). When the amount of added *Nt*-WT RNA was ≥5%, an additional peak in the

426   sequence chromatogram appeared (Figure 10C), revealing the presence of the heterogeneous

427   *atpB* mRNA population. Absence of the double peak from the *atpB* sequences of the *Oenothera*

428   I-iota mutant and the analogous transplastomic tobacco lines indicates that the level of RNA

429   polymerase stuttering, if occurring at all, is below the 5% detection threshold. Given that the

430   ATP synthase activity in the mutants reaches levels of more than 17% [in *Nt*-IM14 (+2A);

431   Figures 8D and 9B], frameshift correction must occur mostly, if not exclusively, by ribosome

432   frameshifting.

433

Discussion

435   Plastome mutants are an important tool for the analysis of non-Mendelian inheritance, the study

436   of photosynthesis, and the analysis of the mechanisms of chloroplast gene expression (Greiner,

437   2012; Sobanski et al., 2019). Frameshift mutations usually lead to disruption of protein function,

438   unless they are transcriptionally or translationally compensated (Ketteler, 2012; Atkins et al.,

439   2016). Although such recoding is believed to exist in almost all organisms, only very few

440   examples have been found in plants to date (see Introduction).

441

Efficient recoding requires a homopolymeric sequence

443   Recoding based on transcriptional slippage relies on homopolymeric sequences (Baranov et al.,

444   2005), while PRF can occur on either homopolymeric or heteropolymeric slip sites (Baranov et

445   al., 2011). Transplastomic tobacco plants, where in addition to the frameshift mutation, adenines

446   at the third codon position of the oligoA stretch had been replaced by guanines, resulted in white

447   plants [*Nt*-IM13 (AAG+1); Figure 5B], suggesting complete loss of ATP synthase (Hager, 2002;

448   Schmitz-Linneweber et al., 2005). Strongly reduced translation efficiency of these constructs was

449   also observed with the dual-luciferase assay in *E. coli* (Figure 7). These findings indicate that

450   frameshift compensation in *atpB* requires a homopolymeric tract. It was shown in bacteria that

451   mRNAs encoding iterated lysine codons (either AAA or AAG) differ remarkably in efficiency

452   and accuracy of protein synthesis. The presence of repetitive AAA codons reduced protein

453   expression compared to the presence of synonymous AAG codons. This is because 70S

454   ribosomes read AAA and AAG codons differently. Ribosomes that encounter multiple AAA

455   codons undergo sliding, whereas no sliding occurs on AAG codons (Koutmou et al., 2015).

456   These findings are in line with our observation that, in the dual-luciferase assay, an enhanced

457   translation efficiency was detected in pEK4-*Nt*-IM11 (AAG) compared to the wild-type

458   sequence that carries the oligoA stretch [pEK4-*Nt*-WT] (Figure 7).

459   Interestingly, the -2A deletion [*Nt*-IM18 (-2A)] results in an albino phenotype with rare

460   green spots (Figure 8B, Figure 6C). *Nt*-IM18 (-2A) plants are phenotypically more similar to *Nt*-

461   IM13 (AAG+1), and no AtpB peptides were detected in *Nt*-IM18 (-2A). This indicates that -2 or

462   +1 ribosomal frameshifting are not active in chloroplasts (Table 1), and an A_8 homopolymeric

463   tract is also insufficient to effectively induce transcriptional slippage. This is not entirely

464   unexpected in that the propensity of RNA polymerase to stutter is known to be strongly

465   correlated with the length of the (homopolymeric) slippery site (Lin et al., 2015).

466

What mechanism of recoding is acting in I-iota and transplastomic tobacco lines?

468   It can be challenging to distinguish between transcriptional slippage and PRF when monitoring it

469   at a low level (Atkins et al., 2016). PRF often results in the formation of more than one protein.

470   Likely due to instability of the truncated AtpB protein (Nishimura et al., 2017), our proteomic

471   analyses detected only peptides corresponding to the corrected reading frame. However, two

472   corrected protein variants (-1 and +2) were found for *Nt*-IM14 (+2A) (Figure 8F), lending

473   circumstantial support to the operation of ribosomal frameshifting rather than RNA polymerase

474   stuttering. Analysis of the predicted mRNA secondary structure revealed the presence of a stem-

475   loop-type structure downstream the oligoA stretch that can serve as slip site for the ribosome

476   (Figures 3C and 4B).

477   We have assessed the possibility of transcriptional slippage by cDNA analysis of the

478   various mutants. No indication of transcriptional slippage for *Nt*-IM12 (+1A) and I-iota (+1A)

479   (Figure 10A,B) was obtained, but spike-in experiments mixing of *Nt*-IM12 (+1A) or I-iota (+1)

480 with the corresponding wild-type RNAs revealed a detection limit of approximately 15%
481 (Supplemental Figure 2). Since the frame correction in *Nt*-IM12 (+1A) is estimated to be below
482 10% (Figure 5D), the operation of transcriptional slippage cannot be definitively excluded for
483 *Nt*-IM12 (+1A).

484 Strikingly, in the transplastomic tobacco mutants, the +2A insertion into the oligoA tract
485 is more efficiently compensated than the +1A insertion [*Nt*-IM14 (+2A) vs. *Nt*-IM12 (+1A),
486 Figures 8B and 5B]. *Nt*-IM14 (+2A) plants are phenotypically most similar to wild type under
487 mixotrophic conditions, and also can grow photoautotrophically and produce seeds (Figures 8B
488 and 9A). Regarding their photosynthetic parameters, *Nt*-IM14 (+2A) plants display an
489 intermediate phenotype between the wild type and *Nt*-IM12 (+1A) plants (Figures 8C and 9C,
490 Table 3). In *Nt*-IM14 (+2A) plants, AtpB peptides with two or three lysines were detected,
491 suggesting two modes of correction: +2 and -1 (Figure 8F). In other systems, several cases have
492 been reported, where two different ribosomal frameshifts can occur at the same site (Caliskan et
493 al., 2017; Li et al., 2019). As for *Nt*-IM12 (+1A), cDNA analysis revealed no indication of
494 transcriptional slippage in *Nt*-IM14 (+2A) plants (Figure 10A). Importantly, in the cDNA
495 sensitivity test, 5% of added RNA was detectable, when wild type and *Nt*-IM14 (+2A) RNAs
496 were mixed (Figure 10C). Together with the absence of detectable RNA polymerase stuttering,
497 this high sensitivity suggests that the correction occurs at the level of translation (i.e., by PRF).
498 Work in microbial systems has revealed that the efficiency of alternative decoding can be highly
499 variable, ranging from a few percent to up to 80% (Baranov et al., 2005; Caliskan et al., 2015).
500 The frameshifting efficiency in *Nt*-IM14 (+2A) measured by the dual-luciferase reporter assay in
501 *E. coli* was approximately 40% (Figure 7). The efficiency *in planta* may be lower, as evidenced
502 by the measured ATP synthase activity in *Nt*-IM14 (+2A) plants, which was 18% of the activity
503 in wild-type plants (Figures 8D and 9B).

504

505 *Functional significance of recoding in chloroplasts*
506 In plastid genomes, homopolymeric nucleotide stretches are hotspots of mutations (Massouh et
507 al., 2016). Homopolymeric tracts are selected against in bacterial genomes, but are retained more
508 frequently in the genomes of endosymbionts. Transcriptional slippage has been proposed to play
509 a critical role in rescuing gene function (Tamas et al., 2008; Wernegreen et al., 2010). Here
510 polymerase stuttering at homopolymeric tracts can be considered as a mutation-compensating

511 mechanism (Tamas et al., 2008). Whether or not transcriptional slippage occurs in chloroplasts
512 and compensates frameshift mutations and/or generates additional transcript diversity, is
513 currently unclear. If it occurs at the oligoA stretch near to 5' end of *atpB*, its frequency is too low
514 to be detected with the sensitivity of cDNA analysis (Figure 10, Supplemental Figure 2).

515 Programmed ribosomal frameshifting results in the formation of additional protein
516 products, but can also correct indels at the level of translation (Ketteler, 2012; Atkins et al.,
517 2016). Usually, ribosomal frameshifting is tightly regulated. Specific metabolites and aminoacyl-
518 tRNA supply can affect the efficiency of ribosomal frameshifting (Ivanov et al., 2000; Caliskan
519 et al., 2017). When we searched for other possible examples of alternative genetic decoding in
520 the chloroplast, a sequence motif in the *cemA* (*ycf10*) gene (coding for an inner envelope protein
521 likely involved in CO_2 uptake) (Rolland et al., 1997) was identified. In contrast to *O. elata*
522 (which was invested here), *O. glazioviana* and *O. parviflora* (*Oenothera* subgenus *Oenothera*) as
523 well as *O. villaricae* and *O. picensis* (*Oenothera* subgenus *Munzia*) contain two ATG codons
524 embedded in an oligoA stretch within the 5' region of *cemA*. The oligoA stretches of the two
525 pairs of species differ by an indel of 3 bp, and only the second ATG is in frame. To be used, the
526 first ATG would require a +1 (+4) or -2 frameshift. Similar to *atpB*, the oligoA stretch could
527 serve as slippery sequence motif for recoding (Greiner et al., 2008). To what extent recoding can
528 result under certain experimental conditions even in gene fusion products, as suggested by the
529 AtpB/AtpE fusion observed by Sears and Herrmann (1985) (also see Results), remains a matter
530 of speculation.

531 Previous reports on the possibility of recoding in plants were based on bioinformatic
532 prediction (Lin et al., 2015; van der Horst et al., 2019), *in vitro* analysis (Napthine et al., 2003) or
533 indirect genetic evidence (Kohl and Bock, 2009). The data presented in this study provide clear
534 genetic and biochemical evidence for the presence of recoding in the chloroplast *atpB* gene both
535 in the spontaneous plastome mutant I-iota of *Oenothera* and a set of transplastomic tobacco
536 plants. Its presence in chloroplasts may be a relic from the bacterial past of the chloroplast (Lin
537 et al., 2015). To what extent the compensation of mutations by frameshifting is dependent upon
538 the environmental conditions and/or the physiological status of the chloroplast, is an interesting
539 question to be addressed in future studies.

540

541 **Material and Methods**

542

Plant material and growth conditions

544 *Oenothera* (evening primrose) wild type (*Oe*-WT; *O. elata* ssp. *hookeri* strain johansen Standard
545 equipped with the chloroplast genome of *O. elata* ssp. *hookeri* strain hookeri de Vries; johansen
546 Standard I-hookdV) and the I-iota mutant (johansen Standard I-iota) were previously described
547 in Massouh et al. (2016) and cultivated according to Greiner and Köhl (2014). In *Oenothera,*
548 photosynthetically incompetent chloroplast mutants can be kept as variegated plants, containing
549 a mixed population of green nursery chloroplasts and mutated plastids. These plants are viable in
550 soil because the green tissue feeds the non-photosynthetic mutant leaf tissue (Figure 1A). The
551 combination of two chloroplast types in one plant is achieved by taking advantage of biparental
552 chloroplast transmission, which is the rule in evening primroses. To this end, a maintainer strain
553 containing green nursery plastids is crossed to the chloroplast mutant. This results in variegated
554 offspring because vegetative sorting (sorting-out) of the two chloroplast types leads to tissues
555 homoplasmic for either green or mutant chloroplasts in the same plant. Biparental transmission
556 of plastids in *Oenothera* displays, however, maternal dominance. Consequently, the F1
557 generation offspring is usually either homoplasmic for the maternal plastome or heteroplasmic
558 for the paternal and maternal plastomes. To increase the frequency of variegated (heteroplasmic)
559 offspring in F1, a johansen Standard line was equipped with the slowly multiplying plastome IV
560 of *O. parviflora* strain atrovirens Standard (IV-atroSt) as green nursery plastome (cf. Sobanski et
561 al., 2019). This line was then used as parent in crosses with the faster multiplying I-iota
562 plastome. Resulting F1 generations display up to 100% variegation for green and mutated
563 plastomes in the progeny. Homoplasmic mutant tissue generated this way was used for molecular
564 and physiological analyses in this work. For details on the genetics, see (Kutzelnigg and Stubbe,
565 1974; Kirk and Telney-Basset, 1978; Stubbe and Herrmann, 1982; Greiner, 2012; Sobanski et
566 al., 2019).

567 For plant growth, *Oenothera* seeds were soaked in water for 12-16 h at 4°C, germinated
568 on wet filter paper at 27°C in the light, followed by seedling transfer to soil. About one month
569 after germination (early rosette stage) plants were vernalized at 4°C for seven days under a 10 h
570 light/14 h dark regime. Plants were then returned to the greenhouse and cultivated under long-
571 day conditions (16 h light, 180-220 μE m^{-2} s^{-1}, 22 °C/8 h dark, 20 °C, humidity 50%).

572   Homoplasmic I-iota plants and wild-type control plants were cultivated in Magenta

573   vessels (Sigma-Aldrich) under aseptic conditions (sterile culture). Seeds were sterilized

574   following a vapor-phase sterilization protocol. Seeds in open microcentrifuge tubes were placed

575   in a desiccator jar together with a glass beaker containing 100 mL of 13% [v/v] NaClO. Prior to

576   sealing the desiccator jar, 3 mL concentrated HCl was carefully added to the bleach. Seeds were

577   then sterilized in developing chlorine fumes for 5 h, followed by seeds ventilation in open tubes

578   in a laminar flow hood for several hours to completely eliminate the chlorine gas. Subsequently,

579   seeds were plated on germination medium containing ½ MS salts (Murashige and Skoog, 1962),

580   0.5% [w/v] Agargel (Sigma Aldrich), and 0.05% [v/v] Plant Preservative Mixture (Plant Cell

581   Technology), adjusted to pH 5.8 with KOH, and incubated for 27°C in the light. After one week,

582   seedlings were transferred to ½ MS medium with Agargel (see above) supplemented with 1.75%

583   [w/v] glucose and cultivated at 16 h light 50 μE m^{-2} s^{-1}/8 h dark and 24 °C.

584   *Nicotiana tabacum* cv. Petit Havana (*Nt*-WT) and *atpB-aadA* control plants (Rott et al.,

585   2011) were raised from seeds in soil under controlled growth conditions (16 h light, 150-180 μE

586   m^{-2} s^{-1}, 25 °C/8 h dark, 20°C; humidity 60%). Transplastomic tobacco lines were cultivated in

587   Magenta boxes on agar-solidified MS medium containing 3% [w/v] sucrose and supplemented

588   with 500 mg/L spectinomycin under 16 h light, 50 μmol m^{-2}s^{-1}/8 h dark, 24 °C. For homoplasmy

589   tests (Svab and Maliga, 1993; Bock, 2001), seeds were surface-sterilized by soaking in 70%

590   [v/v] ethanol for two minutes, followed by soaking in 3% [v/v] NaClO containing a drop of

591   Triton X-100 for 15 minutes. The seeds were then rinsed with sterilized water 5-7 times and

592   plated on MS-based selective media containing 500 mg/L spectinomycin, or 500 mg/L

593   streptomycin (Rott et al., 2011). Homoplasmic *Nt*-IM13 (AAG+1) and *Nt*-IM18 (-2A) seeds

594   were obtained from stable *Nt*-IM13 (AAG+1)/WT and *Nt*-IM18 (-2A)/WT periclinal chimeras

595   (plants with white leaf border carrying mutated chloroplast and green leaf blade with wild-type

596   chloroplasts; cf. Greiner 2012), respectively.

597

598   ***Test for homoplasmic I-iota tissue***

599   Homoplasy of leaf sectors of I-iota was assessed using a sequence length polymorphism in the

600   *clpP* gene that distinguishes the nursery plastome IV-atroSt (GenBank accession number

601   EU262891.2) from the I-iota plastome that derives from I-hookdV (GenBank accession numbers

602 KT881170.1; Massouh et al. 2016). The marker was amplified by standard PCR, employing the

603 primer pair clpP_IvsIV_for and clpP_IvsIV_rev (Supplemental Table 4; cf. Figure 1B).

604

605 *Generation of transplastomic tobacco lines*

606 Point mutations in *atpB* were introduced by site-directed mutagenesis. 177 bp from the 5'-part of

607 *atpB* were cloned into the pEXA vector (Eurofins) and used as a template. Primer pairs used for

608 PCR are listed in Supplemental Table 4. Reactions were carried out employing Phusion High

609 Fidelity DNA polymerase according to the manufacturer's instructions (Thermo Scientific).

610 Non-mutated parental DNA was digested with the restriction enzyme DpnI for 1 h at 37°C.

611 DpnI-treated DNA was transformed into DH5-alpha chemically competent cells and plated on

612 LB medium supplemented with 100 μg mL^{-1} ampicillin. Single colonies were used for

613 inoculation of overnight culture and plasmids isolated with the help of the QIAprep Spin

614 Miniprep Kit (Qiagen). The presence of the mutation was verified by Sanger sequencing (LGC

615 genomics). Positive clones were digested by CpoI and BspOI (Thermo Scientific) and the

616 released *atpB* fragment was ligated into the similarly digested *aadA-atpB* plasmid (Figure 6A;

617 Rott et al., 2011) using T4 ligase (Invitrogen).

618 Transplastomic lines were generated by biolistic transformation (Rott et al., 2011).

619 Several homoplasmic lines were identified after the first regeneration round. Homoplasmy of the

620 lines was verified by restriction fragment length polymorphism (RFLP) analysis (Figure 6B).

621 Point mutations were confirmed by Sanger sequencing (LGC genomics).

622

623 *DNA gel blot and RFLP analyses*

624 Total plant DNA was isolated by a rapid cetyltrimethylammonium bromide-based miniprep

625 method (Doyle, 1990). DNA samples were digested with PvuII and NcoI, separated in 1% [w/v]

626 agarose gels and blotted onto Amersham Hybond-XL membranes (GE Healthcare) according to

627 the supplier's recommendations. Specific probes were generated by PCR amplification (Figure

628 6A, primers are listed in Supplemental Table 4). For hybridization, α [^{32}P] dCTP-labeled probes

629 were generated by random priming (Megaprime DNA labeling kit; GE Healthcare).

630 Hybridization was performed in Church Buffer (1% [w/v] BSA, 1 mM EDTA, 7% [w/v] SDS,

631 0.5 M Na$_2$HPO4/H$_3$PO$_4$, pH 7.2) at 65°C overnight. Subsequently, the membranes were briefly

632 rinsed with Wash Solution I (0.1% [w/v] SDS, 300 mM NaCl, 30 mM sodium citrate), then

633 incubated under continuous agitation in Wash Solution I at room temperature for 20 min, and

634 finally washed twice with Wash Solution II (0.1% [w/v] SDS, 75 mM NaCl, 7.5 mM sodium

635 citrate) for 15 min at 65 °C. For signal detection, the membranes were incubated in

636 phosphorimager cassettes, and the hybridization signals were visualized by scanning in

637 aTyphoon TRIO+ Variable Mode Imager (Amersham Biosciences).

638

639 *Analysis of cDNA*

640 RNA from *Oenothera* and tobacco leaves was extracted with the Spectrum Plant Total RNA kit

641 (Sigma Aldrich). Genomic DNA was eliminated with the Turbo DNA-free kit (Ambion). cDNA

642 was generated with the AccuScript High Fidelity cDNA kit (Agilent) according to the supplier's

643 recommendation and using gene-specific primers (Supplemental Table 4). Phusion High-Fidelity

644 DNA polymerase (ThermoFisher Scientific) was used for subsequent PCR amplification.

645

646 *Prediction of RNA secondary structure*

647 mRNA secondary structures were predicted with the mfold web server (Zuker, 2003).

648

649 *Photosynthesis measurements*

650 Light-response curves of chlorophyll-*a* fluorescence parameters were determined at 22°C using

651 the fiberoptics version of the Dual-PAM instrument (Heinz Walz GmbH). Linear electron flux

652 and the redox state of the PSII acceptor side (qL) (Kramer et al., 2004) were measured after 30

653 min of dark adaptation. Light intensity was stepwise increased from 0 to 2000 μE m^{-2} s^{-1}, with a

654 measuring time for each light intensity of 150 s under light-limited conditions and 60 s under

655 light-saturated conditions. After the measurement, the chlorophyll content and chlorophyll a/b

656 ratio of the measured leaf segment were determined in 80% (v/v) acetone according to (Porra et

657 al., 1989).

658 Proton conductivity of the thylakoid membrane (gH^{+}) was used as a measure of ATP

659 synthase activity. It was determined on intact leaves from the decay kinetics of the

660 electrochromic shift signal (ECS) during a short interval of darkness. The experiments were

661 performed at 22°C. Leaves were pre-illuminated for 5 min with saturating light (1000 μE m^{-2}

662 s^{-1}) so that photosynthesis was fully activated and ATP synthase activity was not limited by ATP

663 consumption by the Calvin–Benson-Bassham cycle. The saturating illumination was interrupted

23

664   by 15 s intervals of darkness, and the rapid first phase of the decay kinetic of the electrochromic

665   shift was fitted with a single exponential decay function. Depending on the mutants measured,

666   this fit was restricted to time intervals between 200 ms [for the wild type *Nt*-WT, *aadA-atpB* and

667   *Nt*-IM11 (AAG)] and a maximum of 800 ms after the end of the actinic illumination [in case of

668   mutants with very low ATP synthase activity such as *Nt*-IM12 (+1A), *Nt*-IM14 (+2A), or *Nt*-

669   IM16 (-1A)]. The reciprocal value of the time constant was used as a measure of ATP synthase

670   activity. Signals were measured and deconvoluted using a KLAS-100 spectrophotometer (Heinz

671   Walz GmbH) as previously described (Rott et al., 2011).

672

673   *Thylakoid isolation*

674   Leaves from 6-8 week-old *Oenothera* plants were harvested in the beginning of the light phase

675   and shortly placed in ice water. 10 g of leave material was mixed with 200 mL Isolation Medium

676   [50 mM HEPES/KOH (pH 7.6), 330 mM sorbitol, 2 mM EDTA, 1 mM $MgCl_2$, 5 mM sodium

677   ascorbate] and blended in a Waring blender (5 times 5 s each). Then, the homogenate was

678   filtered through a double layer of mull and Miracloth (Merck), and the filtrate centrifuged at

679   5.000 g for 5 min at 4°C. Subsequently, the pellet was resuspended with a brush in 40 mL Wash

680   Medium [50 mM HEPES/KOH (pH 7.6), 5 mM sorbitol)], homogenized in a 30 mL potter

681   homogenizer (PYREX) until the chloroplast pellet was dissolved, and centrifuged at 5.000 *g*, 5

682   min, 4°C. The pellet was then again resuspended, homogenized in a potter homogenizer and

683   centrifuged two times as above. Finally, the pellet was resuspended in 5 mL washing medium,

684   layered on top of 85% Percoll solution [85% PBF-Percoll stock solution contains 3% [w/v] PEG

685   6000, 1% [w/v] bovine serum albumin, 1% [w/v] Ficoll 400; 330 mM sorbitol, 50 mM

686   HEPEs/KOH (pH7.6), 2 mM EDTA, 1 mM $MgCl_2$] and centrifuged at 10.000 *g* for 5 min at 4°C.

687   Thylakoids were washed once with Wash Medium (5.000 g, 5 min, 4°C) and resuspended in

688   Storage Buffer [50 mM HEPES/KOH (pH 7.6), 10% [v/v] glycerol, 5 mM $MgCl_2$, 100 mM

689   sorbitol], frozen in liquid N_2 and stored at -80°C until use.

690

691   *Protein isolation and SDS-PAGE*

692   Thylakoids membranes (20 µg chlorophyll equivalent) were pelleted by centrifugation (20,000 *g*,

693   10 min, 4 °C) and resuspended in 30 µL extraction buffer [25 mM BisTris/HCl (pH 7.0), 20%

694   [v/v] glycerol, 0.25 g/l cOmplete protease inhibitor (Roche)]. Plant total proteins were extracted

695   from 20 mg of frozen ground leaf material homogenized in 100 µL of extraction buffer.

696   Membranes were solubilized by addition of 1% [w/v] n-dodecyl-β-D-maltoside (Sigma Aldrich)

697   in the darkness on ice for 5 min. Finally, samples were denatured in Sample Buffer (62 mM

698   Tris/HCl, pH 6.8, 10% [v/v] glycerol, 2% [v/v] sodium dodecyl sulfate) for 3 min at 95°C. SDS

699   polyacrylamide gel electrophoresis with 9% [T] separation gels was performed according to

700   (Laemmli, 1970). After electrophoresis, proteins were visualized by Coomassie staining.

701   Separation gels were incubated in staining solution (0.1% [w/v] Coomassie Blue G, 0.1% [w/v]

702   Coomassie Blue R, 45% [v/v] methanol, 9% [v/v] acetic acid) for 10 min under continuous

703   agitation at room temperature. Gels were destained by incubation in 30% [v/v] methanol, 5%

704   [v/v] acetic acid solution.

705

Western blot analyses

707   Proteins separated by SDS-PAGE were transferred to polyvinylidene difluoride membranes (0.2

708   µm, Thermo Scientific) using a semi-dry electroblotting system (PeqLab). Primary antibodies

709   produced in rabbit against AtpB and AtpE were purchased from Agrisera. As secondary

710   antibody, an anti-rabbit IgG peroxidase conjugate was used (Agrisera). Immunochemical

711   detection was performed using the ECL system (GE Healthcare) according to the supplier's

712   recommendation. Membranes were exposed to an X-ray film (Amersham TM ECL, GE

713   Healthcare). Films were developed using an X-ray film developer (Hyper processor, GE

714   Healthcare).

715

Samples preparation for LC-MS/MS

717   For in-solution digestion, thylakoids from *Oe*-WT and I-iota (50 µg each) were solubilized in

718   UTU buffer (6 M urea/2 M thiourea, pH 8.0) and subsequently incubated in reduction buffer (1

719   µg/µL DTT in ddH$_2$O) for 1 h at 50°C followed by incubation with alkylation buffer (55 mM

720   iodoacetamide in ddH$_2$O) in the dark for 30 min at room temperature. The samples were then

721   treated with endoproteinase Lys-C (0.5 µg/µL 10 mM Tris/HCl, pH 8.0) for four hours at room

722   temperature and digested in 0.4 µg/µL of trypsin (both purchased from Promega) overnight at

723   room temperature. Bovine serum albumin (BSA) was used as a control and treated identically.

724   Digestion was stopped by addition of TFA (0.2% [v/v] final concentration). Peptides were

725   purified using Zip tip C18 pipette tips (Millipore) according to the manufacturer's instructions.

726   For in-gel digestion, SDS–PAGE-separated and Coomassie-stained protein bands were
727   excised from the gel and destained using a mixture of 40% [v/v] acetonitrile and 60% 50 mM
728   [v/v] NH$_4$HCO$_3$ at 37°C under continuous agitation. Gel pieces were dried by vacuum
729   centrifugation and incubated with trypsin (modified sequencing grade, Roche) in 50 mM
730   NH$_4$HCO$_3$ or Glu-C (sequencing grade, Promega) in 50 mM Tris/PO$_4$, pH 7.8 for 12-16 h at 37
731   °C. Proteolytic peptides were extracted by repetitive incubation with acetonitrile, 5% [v/v]
732   formic acid, and again acetonitrile. The combined supernatants were dried by vacuum
733   centrifugation, and peptides from were purified using Zip tip C18 pipette tips (Millipore)
734   according to the manufacturer's instructions.

735

736   *LC-MS/MS*

737   Samples generated by in-solution digestion for quantification of AtpA, AtpB, and AtpE in *Oe*-
738   WT and I-iota were subjected LC-MS/MS with free labeling approach. The peptides were
739   resuspended in 2% (v/v) acetonitrile, 0.1 % (v/v) TFA and injected using nanoflow HPLC
740   (Proxeon Biosystems) into the analytical column (length: 12 cm, diameter: 75 μm) filled with
741   C18 (Reprosil C18; Dr. Maisch GmbH). Peptides were eluted from the column in a 90 minute
742   linear gradient of 5 to 80% acetonitrile at a flow rate of 250 μL/min. Samples were analyzed
743   using the selected reaction monitoring method (SRM). Fragmentation and detection were
744   performed with a TSQ Quantum UltraTM Triple Stage Quadrupole Mass Spectrometer (Thermo
745   Fisher Scientific). Specific peptide sequences unique for the target proteins (AtpA, AtpB, AtpE)
746   were created using the Pinpoint software (version 1.0, Thermo Scientific) and are listed in
747   Supplemental Table 3. Peptides obtained from mass spectrometry were analyzed with the
748   Pinpoint software (Thermo Scientific). The proteomic datasets have been deposited in the
749   ProteomeXchange Consortium (http://www.proteomexchange.org) via the PRIDE partner
750   repository with the dataset identifier PXD020246.

751   Samples generated by in-gel digestion were resuspended in 5% (v/v) acetonitrile and
752   0.1% (v/v) formic acid. Peptides were separated on a C18 reversed-phase analytical column
753   (Acclaim PepMap100, Thermo Fisher Scientific) using an Easy-nLC 1000 liquid
754   chromatography system (Thermo Fisher Scientific). Peptides were eluted in a 28-min-long non-
755   linear 5% - 34% acetonitrile gradient in 0.1% formic acid and 5% DMSO at a flow of 300 nL
756   min^{-1}. Subsequently, the column was cleaned for 10 min with 85% acetonitrile in 0.1% formic

757 acid and 5% DMSO. Eluted peptides were transferred to an NSI source and sprayed into an

758 Orbitrap Q-Exactive Plus mass spectrometer (Thermo Fisher Scientific). The MS was run in

759 positive ion mode. For full MS scans, the following settings were used: resolution: 70000, AGC

760 target: 3E6, maximum injection time: 100 ms, and scan range: 200 to 2000 m/z. For dd-MS^2, the

761 following settings were used: resolution: 175000, AGC target: 1E5, maximum injection time: 50

762 ms, loop count: 15, isolation window: 4.0 m/z, and NCE: 30. In addition, the following data-

763 dependent settings were used: underfill ratio: 1%, apex trigger: off, charge exclusion:

764 unassigned, 1, 5, 5–8, >8, peptide match: preferred, exclude isotypes: on, and dynamic exclusion:

765 20.0 s.

766   The raw files obtained from Xcalibur (Thermo Fisher Scientific) were converted into mgf

767 files using MSConvert from the Proteowizard portal. The files were analyzed by the Mascot

768 server with an in-house database containing protein sequences from several plant species

769 POTbase MS (Moreno et al., 2018), or a database containing the AtpB sequence and the

770 potential variations in lysine content (summarized in Table 1, for sequences see Supplemental

771 Table 1).

772

773

774 *Multiple sequence alignments*

775 ClustalW (Thompson et al., 1994) implemented in the MegAlignPro software (DNAStar) was

776 used to perform multiple sequence alignments. DNA sequences were obtained from NCBI Gene

777 (https://www.ncbi.nlm.nih.gov/gene/). Sequences of *atpB* with the following gene ID were used

778 to generate the alignment: 844757 (*Arabidopsis thaliana*), 29141377 (*Oryza sativa*), 4099984

779 (*Solanum tuberosum*), 845170 (*Zea mays*), 802790 (*Oenothera elata*), and 800515 (*Nicotiana*

780 *tabacum*).

781

782 *Dual-luciferase reporter assay*

783 The dual luciferase reporter plasmid was designed on the basis of the pEK4 vector (Kramer and

784 Farabaugh, 2007). 150 bp from the 5'-region of *atpB* from *N. tabacum* and *O. elata* (GenBank

785 accession numbers Z00044.2 and KT881170.1, respectively) containing the oligoA stretch were

786 cloned into the polylinker of the insertion window of pEK4 using BglII and BamHI restriction

787 sites. Final constructs were transformed into NEB Express chemically competent *E. coli* cells

788   (C3037I, NEB). Cultures of three individual clones were grown at 37°C in LB medium

789   supplemented with 100 μg mL^{-1} of ampicillin. Upon reaching an OD of 0.4, equal volumes of

790   suspension were collected. Crude extracts were prepared according to (Meydan et al., 2017). The

791   activities of firefly and Renilla luciferases were measured using the Dual-Luciferase Reporter

792   Assay System (Promega). Luminescence was followed in 96-well plates in a ClarioStar micro

793   plate reader (BMG Labtech). The PRF efficiency was calculated according to (Grentzmann et al.,

794   1998).

795

796   *Transmission electron microscopy*

797   *Oenothera* leaf pieces of 2 mm^2 were fixed with 2.5% [w/v] glutaraldehyde and 2% [w/v]

798   paraformaldehyde in 0.2 M sodium cacodylate buffer (pH 7.4) for at least 4 h at 4°C. Samples

799   were then post-fixed in 1% [w/v] OsO_4 at 4°C overnight, stained in 2% [w/v] aqueous uranyl

800   acetate for 2 h and dehydrated gradually in 30, 50, 70, 80, 90 and 100% [v/v] ethanol followed

801   by washing in 100% [v/v] propylene oxide two times. The samples were then embedded in low-

802   melting Spurr epoxy resin (Agar Scientific), degassed and cured at 65 °C for 24 h. Thin sections

803   (60-70 nm) were obtained with a Leica Ultracut UC 6 (Leica Microsystems), mounted on 150

804   mesh nickel grids, counterstained with uranyl acetate followed by lead citrate, and examined

805   with a transmission electron microscope at 120 kV (EFTEM, Zeiss).

806

807   **Acknowledgments**

817

818   **Author contribution**:

819   I.M., A.Z., A.M. performed protein analysis (western blot and samples preparation for MS).

820   E.M. and W.S. performed MS analysis. I.M., M.R, L.Y.R., and S.R. generated and identified

821   tobacco transplastomic lines. M.A.S. performed photosynthesis analysis and measured the

822   activity of the ATP synthase. All authors analyzed and discussed the data. I.M. and S.G.

823   designed the study. I.M. wrote the manuscript with significant contribution from S.G., M.A.S

824   and R.B. All authors approved the final version.

References

Anikin M, Molodtsov V, Temiakov D, McAllister WT (2010) Transcript slippage and recoding. *In* JF Atkins, RF Gesteland, eds, Recoding: expansion of decoding rules enriches gene expression. Springer New York, New York, NY, pp 409-432

Arezi B, Hogrefe HH (2007) *Escherichia coli* DNA polymerase III epsilon subunit increases Moloney murine leukemia virus reverse transcriptase fidelity and accuracy of RT-PCR procedures. *Anal Biochem* **360:** 84-91

Atkins JF, Loughran G, Bhatt PR, Firth AE, Baranov PV (2016) Ribosomal frameshifting and transcriptional slippage: From genetic steganography and cryptography to adventitious use. *Nucleic Acids Res* **44:** 7007-7078

Baranov PV, Atkins JF, Yordanova MM (2015) Augmented genetic decoding: global, local and temporal alterations of decoding processes and codon meaning. *Nat Rev Genet* **16:** 517-529

Baranov PV, Fayet O, Hendrix RW, Atkins JF (2006) Recoding in bacteriophages and bacterial IS elements. *Trends Genet* **22:** 174-181

Baranov PV, Hammer AW, Zhou J, Gesteland RF, Atkins JF (2005) Transcriptional slippage in bacteria: distribution in sequenced genomes and utilization in IS element gene expression. *Genome Biol* **6:** R25

Baranov PV, Wills NM, Barriscale KA, Firth AE, Jud MC, Letsou A, Manning G, Atkins JF (2011) Programmed ribosomal frameshifting in the expression of the regulator of intestinal stem cell proliferation, adenomatous polyposis coli (APC). *RNA Biol* **8:** 637-647

Barkan A (2011) Expression of plastid genes: organelle-specific elaborations on a prokaryotic scaffold. *Plant Physiol* **155:** 1520-1532

Belew AT, Dinman JD (2015) Cell cycle control (and more) by programmed -1 ribosomal frameshifting: implications for disease and therapeutics. *Cell Cycle* **14:** 172-178

Bock R (2001) Transgenic plastids in basic research and plant biotechnology. *J Mol Biol* **312:** 425-438

Bock R (2007) Structure, function, and inheritance of plastid genomes. *In* R Bock, ed, Cell and Molecular Biology of Plastids. Springer, Berlin, Heidelberg, New York, pp 29–63

856 **Bock R** (2017) Witnessing genome evolution: experimental reconstruction of endosymbiotic and
857   horizontal gene transfer. *Annu Rev Genet* **51:** 1-22

858 **Bock R, Timmis JN** (2008) Reconstructing evolution: gene transfer from plastids to the nucleus.
859   *Bioessays* **30:** 556-566

860 **Brierley I, Jenner AJ, Inglis SC** (1992) Mutational analysis of the "slippery-sequence"
861   component of a coronavirus ribosomal frameshifting signal. *J Mol Biol* **227:** 463-479

862 **Caliskan N, Peske F, Rodnina MV** (2015) Changed in translation: mRNA recoding by -1
863   programmed ribosomal frameshifting. *Trends Biochem Sci* **40:** 265-274

864 **Caliskan N, Wohlgemuth I, Korniy N, Pearson M, Peske F, Rodnina MV** (2017) Conditional
865   switch between frameshifting regimes upon translation of dnaX mRNA. *Mol Cell* **66:**
866   558-567.e554

867 **Doyle JJ** (1990) Isolation of plant DNA from fresh tissue. *Focus* **12:** 13-15

868 **Gesteland RF, Weiss RB, Atkins JF** (1992) Recoding: reprogrammed genetic decoding.
869   *Science* **257:** 1640-1641

870 **Greiner S** (2012) Plastome mutants of higher plants. *In* R Bock, V Knoop, eds, Genomics of
871   chloroplasts and mitochondria. Springer, Dordrecht, Heidelberg, New York, London, pp
872   237–266

873 **Greiner S, Köhl K** (2014) Growing evening primroses (*Oenothera*). *Front Plant Sci* **5:** 38

874 **Greiner S, Wang X, Rauwolf U, Silber MV, Mayer K, Meurer J, Haberer G, Herrmann**
875   **RG** (2008) The complete nucleotide sequences of the five genetically distinct plastid
876   genomes of *Oenothera*, subsection *Oenothera*: I. sequence evaluation and plastome
877   evolution. *Nucleic Acids Res* **36:** 2366-2378

878 **Grentzmann G, Ingram JA, Kelly PJ, Gesteland RF, Atkins JF** (1998) A dual-luciferase
879   reporter system for studying recoding signals. *RNA* **4:** 479-486

880 **Hager M** (2002) Anwendung reverser Genetic zur Fukntionsanalyse plastidenkodierter Gene.
881   Inaugural-Dissertation. Albert-Ludwigs-Universität Freiburg i. Br.

882 **Hahn A, Vonck J, Mills DJ, Meier T, Kuhlbrandt W** (2018) Structure, mechanism, and
883   regulation of the chloroplast ATP synthase. *Science* **360**

884 **Hausmann S, Garcin D, Delenda C, Kolakofsky D** (1999) The versatility of paramyxovirus
885   RNA polymerase stuttering. *J Virol* **73:** 5568-5576

886 **Herrmann RG** (1997) Eukaryotism, towards a new interpretation. *In*. Springer Berlin
887   Heidelberg, Berlin, Heidelberg, pp 73-118

888 **Herrmann RG, Seyer P, Schedel R, Gordon K, Bisanz C, Winter P, Hildebrandt JW,**
889   **Wlaschek M, Alt J, Driesel AJ, Sears BB** (1980) The plastid chromosomes of several
890   dicotyledons. *In* T Bücher, W Sebald, H Weiss, eds, Biological Chemistry of Organelle
891   Formation. Springer Berlin Heidelberg, Berlin, Heidelberg, pp 97-112

892 **Ivanov IP, Gesteland RF, Atkins JF** (2000) Antizyme expression: a subversion of triplet
893   decoding, which is remarkably conserved by evolution, is a sensor for an autoregulatory
894   circuit. *Nucleic Acids Res* **28:** 3185-3196

895 **Ivanova NN, Schwientek P, Tripp HJ, Rinke C, Pati A, Huntemann M, Visel A, Woyke T,**
896   **Kyrpides NC, Rubin EM** (2014) Stop codon reassignments in the wild. *Science* **344:**
897   909-913

898 **Jacks T, Madhani HD, Masiarz FR, Varmus HE** (1988) Signals for ribosomal frameshifting
899   in the Rous sarcoma virus *gag-pol* region. *Cell* **55:** 447-458

900 **Jacques JP, Hausmann S, Kolakofsky D** (1994) Paramyxovirus mRNA editing leads to G
901   deletions as well as insertions. *EMBO J* **13:** 5496-5503

902 **Jarvis P, López-Juez E** (2013) Biogenesis and homeostasis of chloroplasts and other plastids.
903   *Nat Rev Mol Cell Biol* **14:** 787-802

904 **Karcher D, Bock R** (2002) The amino acid sequence of a plastid protein is developmentally
905   regulated by RNA editing. *J Biol Chem* **277:** 5570-5574

906 **Ketteler R** (2012) On programmed ribosomal frameshifting: the alternative proteomes. *Front*
907   *Genet* **3:** 242

908 **Kirk JTO, Telney-Basset RAE** (1978) The plastids their chemistry, structure, growth and
909   inheritance. Elsevier, Amsterdam/New York/Oxford

910 **Kohl S, Bock R** (2009) Transposition of a bacterial insertion sequence in chloroplasts. *Plant J*
911   **58:** 423-436

912 **Koutmou KS, Schuller AP, Brunelle JL, Radhakrishnan A, Djuranovic S, Green R** (2015)
913   Ribosomes slide on lysine-encoding homopolymeric A stretches. *Elife* **4**

914 **Kramer DM, Johnson G, Kiirats O, Edwards GE** (2004) New fluorescence parameters for the
915   determination of QA redox state and excitation energy fluxes. *Photosynth Res* **79:** 209

916 **Kramer EB, Farabaugh PJ** (2007) The frequency of translational misreading errors in *E. coli* is
917 largely determined by tRNA competition. *RNA* **13:** 87-96

918 **Kurland CG** (1992) Translational accuracy and the fitness of bacteria. *Annu Rev Genet* **26:** 29-
919 50

920 **Kutzelnigg H, Stubbe W** (1974) Investigation on plastome mutants in *Oenothera*: 1. General
921 considerations. *Subcell. Biochem* **3:** 73-89

922 **Laemmli UK** (1970) Cleavage of structural proteins during the assembly of the head of
923 bacteriophage T4. *Nature* **227:** 680-685

924 **Landau AM, Lokstein H, Scheller HV, Lainez V, Maldonado S, Prina AR** (2009) A
925 cytoplasmically inherited barley mutant is defective in photosystem I assembly due to a
926 temperature-sensitive defect in *ycf3* splicing. *Plant Physiol* **151:** 1802-1811

927 **Larsen B, Wills NM, Nelson C, Atkins JF, Gesteland RF** (2000) Nonlinearity in genetic
928 decoding: homologous DNA replicase genes use alternatives of transcriptional slippage
929 or translational frameshifting. *Proc. Natl. Acad. Sci. USA* **97:** 1683-1688

930 **Li Y, Firth AE, Brierley I, Cai Y, Napthine S, Wang T, Yan X, Kuhn JH, Fang Y** (2019)
931 Programmed -2/-1 ribosomal frameshifting in simarteriviruses: an evolutionarily
932 conserved mechanism. *J Virol* **93**

933 **Lin C-P, Ko C-Y, Kuo C-I, Liu M-S, Schafleitner R, Chen L-FO** (2015) Transcriptional
934 slippage and RNA editing increase the diversity of transcripts in chloroplasts: insight
935 from deep sequencing of Vigna radiata genome and transcriptome. *PloS One* **10:**
936 e0129396-e0129396

937 **Linton MF, Pierotti V, Young SG** (1992) Reading-frame restoration with an apolipoprotein B
938 gene frameshift mutation. *Proc. Natl. Acad. Sci. USA* **89:** 11431-11435

939 **Massouh A, Schubert J, Yaneva-Roder L, Ulbricht-Jones ES, Zupok A, Johnson MT,**
940 **Wright SI, Pellizzer T, Sobanski J, Bock R, Greiner S** (2016) Spontaneous chloroplast
941 mutants mostly occur by replication slippage and show a biased pattern in the plastome of
942 *Oenothera*. *Plant Cell* **28:** 911-929

943 **McCutcheon JP, McDonald BR, Moran NA** (2009) Origin of an alternative genetic code in the
944 extremely small and GC-rich genome of a bacterial symbiont. *PLoS Genet* **5:** e1000565

945 **Meydan S, Klepacki D, Karthikeyan S, Margus T, Thomas P, Jones JE, Khan Y, Briggs J,**
946 **Dinman JD, Vazquez-Laslop N, Mankin AS** (2017) Programmed ribosomal

frameshifting generates a copper transporter and a copper chaperone from the same gene. *Mol Cell* **65:** 207-219

Miller WA, Giedroc DP (2010) Ribosomal frameshifting in decoding plant viral RNAs. *In* GR Atkins J., ed, Recoding: expansion of decoding rules enriches gene expression, Vol Nucleic Acids and Molecular Biology. Springer, New York, NY

Moreno JC, Martinez-Jaime S, Schwartzmann J, Karcher D, Tillich M, Graf A, Bock R (2018) Temporal proteomics of inducible RNAi lines of Clp protease subunits identifies putative protease substrates. *Plant Physiol* **176:** 1485-1508

Murashige T, Skoog F (1962) A revised medium for rapid growth and bio assays with tobacco tissue cultures. *Physiol Plantarum* **15:** 473-497

Namy O, Moran SJ, Stuart DI, Gilbert RJ, Brierley I (2006) A mechanical explanation of RNA pseudoknot function in programmed ribosomal frameshifting. *Nature* **441:** 244-247

Napthine S, Vidakovic M, Girnary R, Namy O, Brierley I (2003) Prokaryotic-style frameshifting in a plant translation system: conservation of an unusual single-tRNA slippage event. *EMBO J* **22:** 3941-3950

Nishimura K, Kato Y, Sakamoto W (2017) Essentials of proteolytic machineries in chloroplasts. *Mol Plant* **10:** 4-19

Nishio JN, Whitmarsh J (1993) Dissipation of the proton electrochemical potential in intact chloroplasts (II. The pH gradient monitored by cytochrome f reduction kinetics). *Plant Physiol* **101:** 89-96

Olspert A, Chung BY, Atkins JF, Carr JP, Firth AE (2015) Transcriptional slippage in the positive-sense RNA virus family Potyviridae. *EMBO Rep* **16:** 995-1004

Parker J (1989) Errors and alternatives in reading the universal genetic code. *Microbiol Rev* **53:** 273-298

Peled-Zehavi HD, A. (2007) Translation and translational regulation in chloroplasts. *In* R Bock, ed, Cell and Molecular Biology of Plastids. Springer-Verlag, Berlin, pp 249–281

Polard P, Prere MF, Chandler M, Fayet O (1991) Programmed translational frameshifting and initiation at an AUU codon in gene expression of bacterial insertion sequence IS911. *J Mol Biol* **222:** 465-477

Porra R, Thompson W, Kriedermann P (1989) Determination of accurate extinction coefficient and simultaneous equations for essaying chlorophylls *a* and *b* extracted with

978   four different solvents: verification of the concentration of chlorophyll standards by

979   atomic absorption spectroscopy. *Biochim Biophys Acta* **975:** 384–394

980 **Ratinier M, Boulant S, Combet C, Targett-Adams P, McLauchlan J, Lavergne JP** (2008)

981   Transcriptional slippage prompts recoding in alternate reading frames in the hepatitis C

982   virus (HCV) core sequence from strain HCV-1. *J Gen Virol* **89:** 1569-1578

983 **Roberts JD, Bebenek K, Kunkel TA** (1988) The accuracy of reverse transcriptase from HIV-1.

984   *Science* **242:** 1171-1173

985 **Rolland N, Dorne AJ, Amoroso G, Sultemeyer DF, Joyard J, Rochaix JD** (1997) Disruption

986   of the plastid ycf10 open reading frame affects uptake of inorganic carbon in the

987   chloroplast of Chlamydomonas. EMBO J **16:** 6713-6726

988 **Rott M, Martins NF, Thiele W, Lein W, Bock R, Kramer DM, Schottler MA** (2011) ATP

989   synthase repression in tobacco restricts photosynthetic electron transport, CO_2

990   assimilation, and plant growth by overacidification of the thylakoid lumen. *Plant Cell* **23:**

991   304-321

992 **Schaffner C, Laasch H, Hagemann R** (1995) Detection of point mutations in chloroplast genes

993   of Antirrhinum majus L. I. Identification of a point mutation in the psaB gene of a

994   photosystem I plastome mutant. *Mol Gen Genet* **249:** 533-544

995 **Schmitz-Linneweber C, Kushnir S, Babiychuk E, Poltnigg P, Herrmann RG, Maier RM**

996   (2005) Pigment deficiency in nightshade/tobacco cybrids is caused by the failure to edit

997   the plastid ATPase alpha-subunit mRNA. *Plant Cell* **17:** 1815-1828

998 **Schöttler MA, Tóth SZ, Boulouis A, Kahlau S** (2015) Photosynthetic complex stoichiometry

999   dynamics in higher plants: biogenesis, function, and turnover of ATP synthase and the

1000   cytochrome b6f complex. *J Exp Bot* **66:** 2373-2400

1001 **Sears BB, Herrmann RG** (1985) Plastome mutation affecting the chloroplast ATP synthase

1002   involves a post-transcriptional defect. *Curr Genet* **9:** 521-528

1003 **Sobanski J, Giavalisco P, Fischer A, Kreiner JM, Walther D, Schöttler MA, Pellizzer T,**

1004   **Golczyk H, Obata T, Bock R, Sears BB, Greiner S** (2019) Chloroplast competition is

1005   controlled by lipid biosynthesis in evening primroses. *Proc. Natl. Acad. Sci. USA* **116:**

1006   5665-5674

1007 **Stubbe W, Herrmann RG** (1982) Selection and maintenance of plastome mutants and

1008   interspecific genome/plastome hybrids from *Oenothera*. *In* HR Edelman M, Chua N-H,

1009   ed, Methods in chloroplast molecular biology. Elsevier, Amsterdam/New York/Oxford,

1010   pp 149–165

1011   **Su HJ, Barkman TJ, Hao W, Jones SS, Naumann J, Skippington E, Wafula EK, Hu JM,**

1012   **Palmer JD, dePamphilis CW** (2019) Novel genetic code and record-setting AT-richness

1013   in the highly reduced plastid genome of the holoparasitic plant Balanophora. *Proc. Natl.*

1014   *Acad. Sci. USA* **116:** 934-943

1015   **Svab Z, Maliga P** (1993) High-frequency plastid transformation in tobacco by selection for a

1016   chimeric aadA gene. *Proc. Natl. Acad. Sci. USA* **90:** 913-917

1017   **Tamas I, Wernegreen JJ, Nystedt B, Kauppinen SN, Darby AC, Gomez-Valero L, Lundin**

1018   **D, Poole AM, Andersson SG** (2008) Endosymbiont gene functions impaired and

1019   rescued by polymerase infidelity at poly(A) tracts. *Proc. Natl. Acad. Sci. USA* **105:**

1020   14934-14939

1021   **Thompson JD, Higgins DG, Gibson TJ** (1994) CLUSTAL W: improving the sensitivity of

1022   progressive multiple sequence alignment through sequence weighting, position-specific

1023   gap penalties and weight matrix choice. *Nucleic Acids Res* **22:** 4673-4680

1024   **Timmis JN, Ayliffe MA, Huang CY, Martin W** (2004) Endosymbiotic gene transfer: organelle

1025   genomes forge eukaryotic chromosomes. *Nat Rev Genet* **5:** 123-135

1026   **Tsiatsiani L, Heck AJ** (2015) Proteomics beyond trypsin. *FEBS J* **282:** 2612-2626

1027   **van der Horst S, Snel B, Hanson J, Smeekens S** (2019) Novel pipeline identifies new upstream

1028   ORFs and non-AUG initiating main ORFs with conserved amino acid sequences in the 5'

1029   leader of mRNAs in *Arabidopsis thaliana*. *RNA* **25:** 292-304

1030   **Vögele K, Schwartz E, Welz C, Schiltz E, Rak B** (1991) High-level ribosomal frameshifting

1031   directs the synthesis of IS150 gene products. *Nucleic Acids Res* **19:** 4377-4385

1032   **Volchkov VE, Becker S, Volchkova VA, Ternovoj VA, Kotov AN, Netesov SV, Klenk HD**

1033   (1995) GP mRNA of Ebola virus is edited by the Ebola virus polymerase and by T7 and

1034   vaccinia virus polymerases. *Virology* **214:** 421-430

1035   **Wernegreen JJ, Kauppinen SN, Degnan PH** (2010) Slip into something more functional:

1036   selection maintains ancient frameshifts in homopolymeric sequences. *Mol Biol Evol* **27:**

1037   833-839

1038 **Yamao F, Muto A, Kawauchi Y, Iwami M, Iwagami S, Azumi Y, Osawa S** (1985) UGA is

1039   read as tryptophan in Mycoplasma capricolum. *Proc. Natl. Acad. Sci. USA* **82:** 2306-

1040   2309

1041 **Zoschke R, Bock R** (2018) Chloroplast translation: structural and functional organization,

1042   operational control, and regulation. *Plant Cell* **30:** 745-770

1043 **Zoschke R, Kroeger T, Belcher S, Schöttler MA, Barkan A, Schmitz-Linneweber C** (2012)

1044   The pentatricopeptide repeat-SMR protein ATP4 promotes translation of the chloroplast

1045   atpB/E mRNA. *Plant J* **72:** 547-558

1046 **Zuker M** (2003) Mfold web server for nucleic acid folding and hybridization prediction. *Nucleic*

1047   *Acids Res* **31:** 3406-3415

1048

Table 1. Possibility space of correction by recoding in Oe*nothera* **I-iota and tobacco transplastomic lines.** The lysine stretch affected by the

mutation is highlighted in grey. Blue letters indicate amino acids expected to deviate from the wild-type sequence according to the standard rules

of genetic decoding. Premature stop codons are highlighted in red.

Species	Genotype	Correction	5' amino acid sequence of AtpB
Oenothera	*Oe*-WT	-	MRINPTTSGPGVSTLEKKK-SGRIAQIIGPVLDVTFPPGKMPNIYNALVVKG[...]
	I-iota (+1A)	-	MRINPTTSGPGVSTLEKKKIGPYRSNHWSSTGCNLSPGEDA**stop**
		+1	MRINPTTSGPGVSTLEKKK-SGRIAQIIGPVLDVTFPPGKMPNIYNALVVKG[...]
		+4	MRINPTTSGPGVSTLEKK--SGRIAQIIGPVLDVTFPPGKMPNIYNALVVKG[...]
		-2	MRINPTTSGPGVSTLEKKKKSGRIAQIIGPVLDVTFPPGKMPNIYNALVVKG[...]
tobacco	*Nt*-WT	-	MRINPTTSGSGVSTLEKK-NPGRVVQIIGPVLDVAFPPGKMPNIYNALVVQG[...]
	aadA-atpB	-	MRINPTTSGSGVSTLEKK-NPGRVVQIIGPVLDVAFPPGKMPNIYNALVVQG[...]
	Nt-IM11 (AAG±0)	-	MRINPTTSGSGVSTLEKK-NPGRVVQIIGPVLDVAFPPGKMPNIYNALVVQG[...]
	Nt-IM12 (+1A)	-	MRINPTTSGSGVSTLEKKKPGACRPNHRSGTRCSLSPGQDAEYL**stop**
		+1	MRINPTTSGSGVSTLEKK-NPGRVVQIIGPVLDVAFPPGKMPNIYNALVVQG[...]
		+4	MRINPTTSGSGVSTLEK--NPGRVVQIIGPVLDVAFPPGKMPNIYNALVVQG[...]
		-2	MRINPTTSGSGVSTLEKKKKNPGRVVQIIGPVLDVAFPPGKMPNIYNALVVQG[...]
	Nt-IM13 (AAG+1)	-	MRINPTTSGSGVSTLEKKKPGACRPNHRSGTRCSLSPGQDAEYL**stop**
		+1	MRINPTTSGSGVSTLEKK-NPGRVVQIIGPVLDVAFPPGKMPNIYNALVVQG[...]
		+4	MRINPTTSGSGVSTLEK--NPGRVVQIIGPVLDVAFPPGKMPNIYNALVVQG[...]
		-2	MRINPTTSGSGVSTLEKKKKNPGRVVQIIGPVLDVAFPPGKMPNIYNALVVQG[...]
	Nt-IM14 (+2A)	-	MRINPTTSGSGVSTLEKKKTRGVSSKSSVRY**stop**
		+2	MRINPTTSGSGVSTLEKK-NPGRVVQIIGPVLDVAFPPGKMPNIYNALVVQG[...]
		-1	MRINPTTSGSGVSTLEKKKKNPGRVVQIIGPVLDVAFPPGKMPNIYNALVVQG[...]
	Nt-IM16 (-1A)	-	MRINPTTSGSGVSTLEKKTRGVSSKSSVRY**stop**
		-1	MRINPTTSGSGVSTLEKK-NPGRVVQIIGPVLDVAFPPGKMPNIYNALVVQG[...]
		-4	MRINPTTSGSGVSTLEKKKNPGRVVQIIGPVLDVAFPPGKMPNIYNALVVQG[...]
	Nt-IM18 (-2A)	-	MRINPTTSGSGVSTLEKKPGACRPNHRSGTRCSLSPGQDAEYL**stop**
		-2	MRINPTTSGSGVSTLEKK-NPGRVVQIIGPVLDVAFPPGKMPNIYNALVVQG[...]
		+1	MRINPTTSGSGVSTLEK--NPGRVVQIIGPVLDVAFPPGKMPNIYNALVVQG[...]

1053 **Table 2.** Identification of AtpB in *Oenothera* I-iota and transplastomic tobacco lines and the

1054 corresponding wild-type and control lines by in-gel tryptic digestion followed by LC MS/MS

1055 analysis. n.d. – not detected.

1056

Genotype	№ of significant matches	№ of significant sequences
Oe-WT	556	26
I-iota (+1A)	113	14
Nt-WT	249	34
aadA-atpB	77	24
Nt-IM11 (AAG±0)	155	31
Nt-IM12 (+1)	28	13
Nt-IM13 (AAG+1)	n.d.	n.d.
Nt-IM14 (+2A)	23	19
Nt-IM16 (-1A)	10	8
Nt-IM18 (-2A)	6	5

Table 3. Analysis of photosynthetic parameters. 3-5 plants were analyzed for both wild types (*Oe*-WT and *Nt*-WT), the I-iota (+1) mutant and the generated transplastomic tobacco lines. For each construct, at least two independent transplastomic lines were analyzed. Because no significant differences between these lines were observed, average data are shown for each genotype. Values are mean ± SD (n=3-5). Letters indicate samples that were not significantly different ($p < 0.05$) according to one-way ANOVA with Holm-Sidak post-hoc testing. ANOVA test was performed separately for greenhouse- and sterile culture-grown plants.

Growth conditions	Genotype	Chlorophyll [mg m^{-2}]	Chlorophyll *a/b*	F_V/F_M
Greenhouse	*Oe*-WT	570.3 ± 12.8[a]	3.6 ± 0.1[a]	0.79 ± 0.01[a]
	I-iota (+1A)	137.5 ± 51.2[b]	2.7 ± 0.2[b]	0.64 ± 0.02[b]
	Nt-WT	438.4 ± 36.0[c]	4.0 ± 0.2[a]	0.83 ± 0.01[a]
	aadA-atpB	414.7 ± 38.5[c]	3.9 ± 0.1[a]	0.81 ± 0.02[a]
	Nt-IM11(AAG)	451.0 ± 23.5[c]	3.8 ± 0.2[a]	0.83 ± 0.01[a]
	Nt-IM14 (+2A)	128.5 ± 17.0[b]	2.6 ± 0.2[b]	0.53 ± 0.08[c]
Sterile culture	*Nt*-WT	297.3 ± 87.0[ab]	3.50 ± 0.24[a]	0.79 ± 0.04[a]
	aadA-atpB	262.8 ± 47. 9[a]	3.42 ± 0.13[a]	0.77 ± 0.03[a]
	Nt-IM11 (AAG)	257.2 ± 63.1[a]	3.50 ± 0.12[a]	0.79 ± 0.03[a]
	Nt-IM12 (+1A)	243.5 ± 70.1[a]	2.34 ± 0.27[b]	0.33 ± 0.14[b]
	Nt-IM14 (+2A)	372.9 ± 78.1[b]	2.78 ± 0.21[c]	0.64 ± 0.18[c]
	Nt-IM16 (-1A)	240.4 ± 95.7[a]	2.17 ± 0.36[b]	0.44 ± 0.23[b]
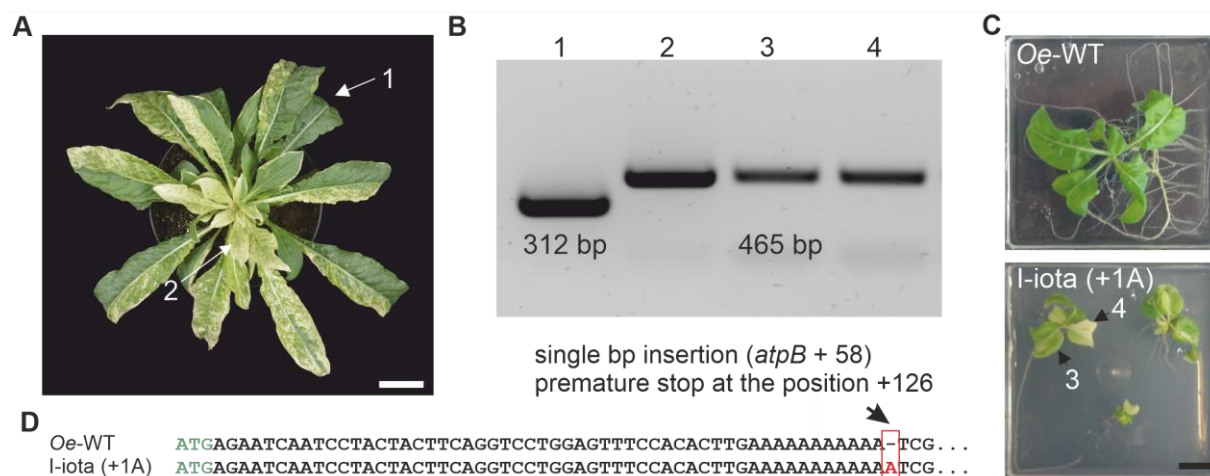
Figure 1. Phenotype and genotype of the I-iota mutant. A. Variegated *Oenothera* plant at the mature rosette stage (seven weeks old) carrying homoplasmic sectors containing the nursery plastome (green) [1] and homoplasmic sectors with I-iota chloroplasts (mottled) [2]. Scale bar: 5cm **B.** PCR confirming homoplasmy of mottled and green sectors (1: nursery plastome [312 bp], 2-4: I-iota plastome [465 bp]; note the absence of the 312 bp band inform lanes 2-4). **C.** Phenotype of wild type (*Oe*-WT) and I-iota homoplasmic plants cultivated under mixotrophic conditions in sterile culture. Lanes 3 and 4 in panel B confirm homoplamsy of the mottled plants. Scale bar: 1cm. **D**. 5' part of the *atpB* gene of *Oe*-WT and I-iota (+1). The mutation at position +58 in an oligoA stretch of *atpB* in I-iota is framed in red. Green letters indicate the start codon.
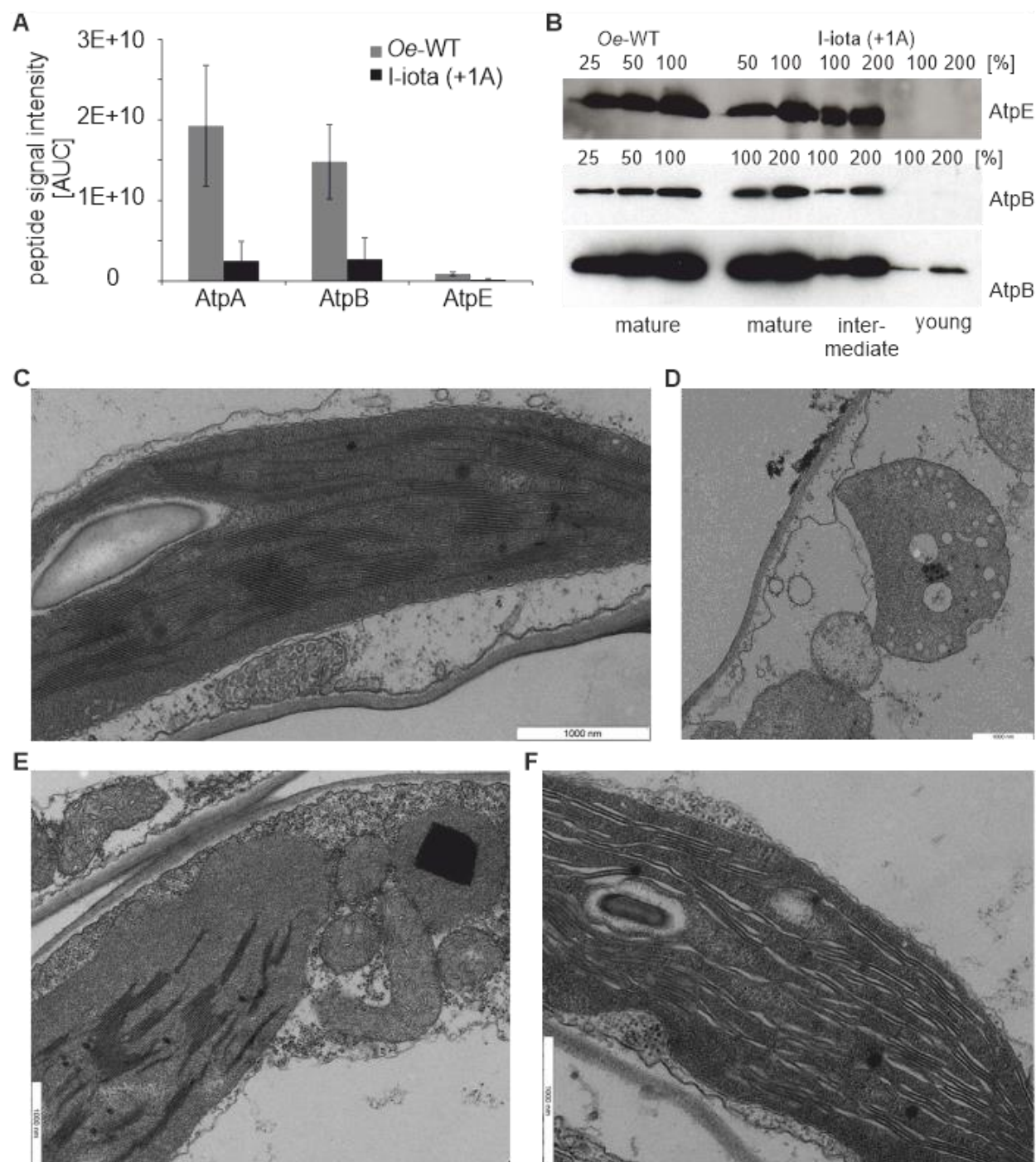
Figure 2. Analysis of ATP synthase and chloroplast ultrastructure in the I-iota mutant and the wild type. A. MS quantification of ATP synthase subunits in wild type and I-iota leaves (n=3). Signal intensities of peptides (AUC: area under the curve) of analyzed protein subunits, were normalized to BSA, which was used as internal control. **B.** Immunoblot detection of AtpE (14.5 kDa) and AtpB (ca. 53 kDa) in thylakoids from the wild type (*Oe*-WT) and I-iota leaves.

Thylakoids were isolated from leaves of 6-8 week-old plants. For the I-iota mutant, leaf tissues of different ages were analyzed (young: top leaves of the rosette, intermediate: mottled leaves from the middle of the rosette, mature: greenish part of leaves from the base of the rosette; see Fig. 1A). Isolated thylakoids were tested for homoplasmy using the *clpP* marker prior to further analysis (see Fig. 1B). Thylakoids were loaded on the basis of the chlorophyll content, with 100% corresponding to 7 µg chlorophyll. The bottom panel (AtpB) shows a longer exposure of the same blot. **C-F**. TEM analysis of wild type [*Oe*-WT] and I-iota leaf tissue. **C**. Wild-type chloroplast. **D-F**. I-iota chloroplasts. **D**. Proplastid-like chloroplast. **E**. Chloroplast with developing thylakoid membrane. **F**. Mature wild type-like chloroplast. 7-week-old plants were investigated.
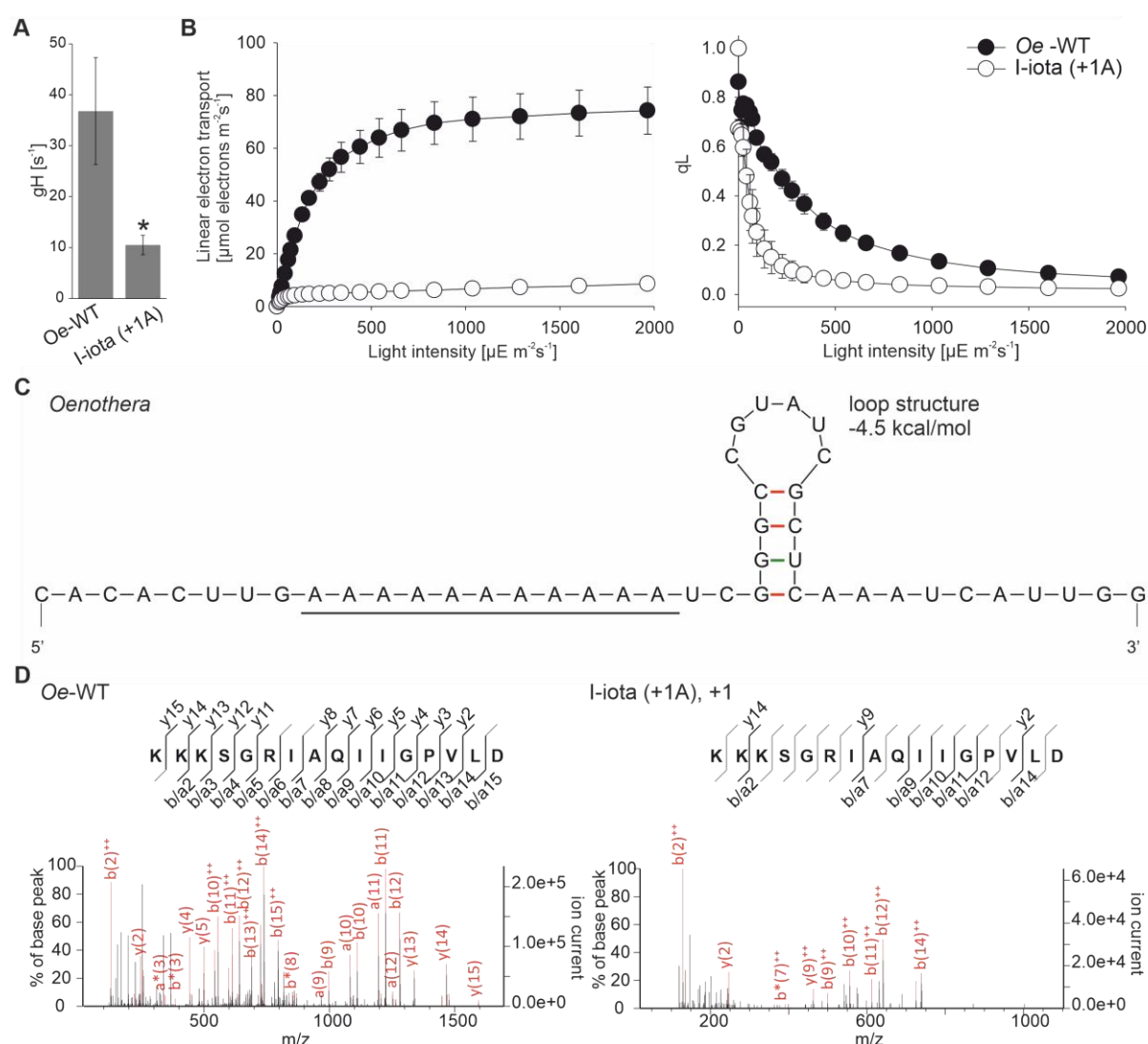
Figure 3. Photosynthetic parameters and analysis of target peptides in in the I-iota mutant and the wild type. A. ATP synthase activity determined from dark-interval decay kinetics of the proton motive force-related electrochromic shift signal. The asterisk indicates a significant difference compared to the wild type (t-test, $p < 0.01$, n=3-5). **B**. Light-response curves of linear electron flux (left panel) and chlorophyll-a fluorescence parameter qL (a measure of the redox state of the PSII acceptor side; right panel) in the wild type [Oe-Wt] and I-iota. 8 wild-type plants and 10 mutant plants were measured. Error bars represent the standard deviation. **C.** Predicted mRNA secondary structure of $atpB$ near the slip site (oligoA stretch; underlined). **D.** LC-MS/MS fragmentation spectrum of the targeted AtpB peptide. The KKK stretch encoded at the slip site is identified as 'b−' and 'y−' type fragment ions.
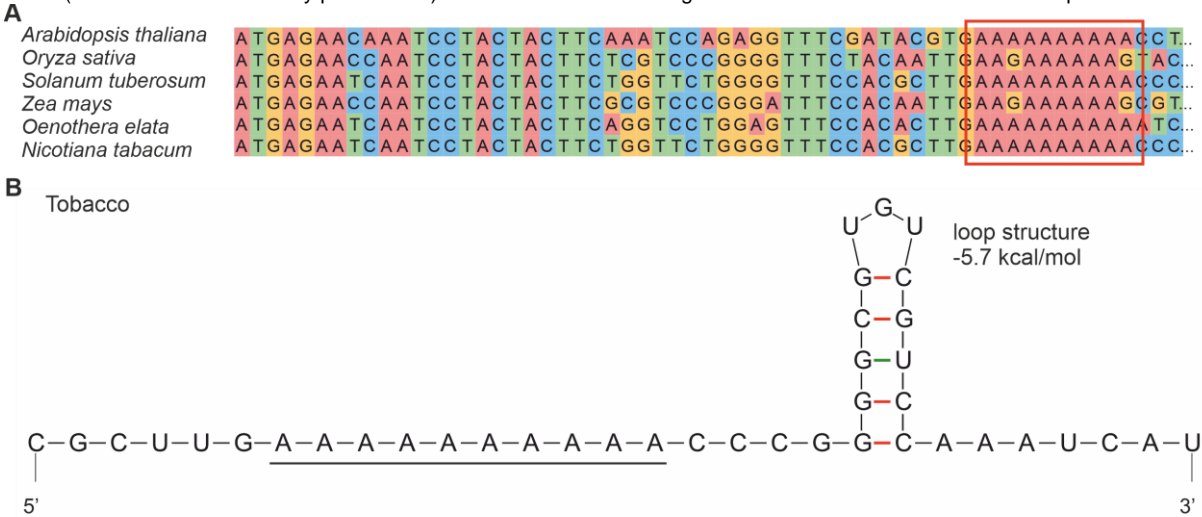
Figure 4. Sequence conservation and folding of the 5' parts of the *atpB* coding region in different species. A. Alignment of the 5'part of the *atpB* coding region in higher plants. Note that all species have an oligopurine motif at the site where slippage occurs in *Oenothera*. the homopolymeric oligoA stretch (boxed in red) is conserved in *Arabidopsis thaliana*, *Solanum tuberosum*, *Oenothera elata*, and *Nicotiana tabacum*. **B.** Predicted mRNA secondary structure of *atpB* near the slip site (oligoA stretch; underlined) in tobacco.

A

```
Nt-WT            ATGAGAATCAATCCTACTACTTCTGGTTCTGGGGTTTCCACGCTTGAAAAAAAAAA--C...
Nt-IM11 (AAG)    ATGAGAATCAATCCTACTACTTCTGGTTCTGGGGTTTCCACGCTTGAGAAGAAGAA--C...
Nt-IM12 (+1A)    ATGAGAATCAATCCTACTACTTCTGGTTCTGGGGTTTCCACGCTTGAAAAAAAAAAA-C...
Nt-IM13 (AAG+1A) ATGAGAATCAATCCTACTACTTCTGGTTCTGGGGTTTCCACGCTTGAGAAGAAGAAA-C...
```

B

C

D

E
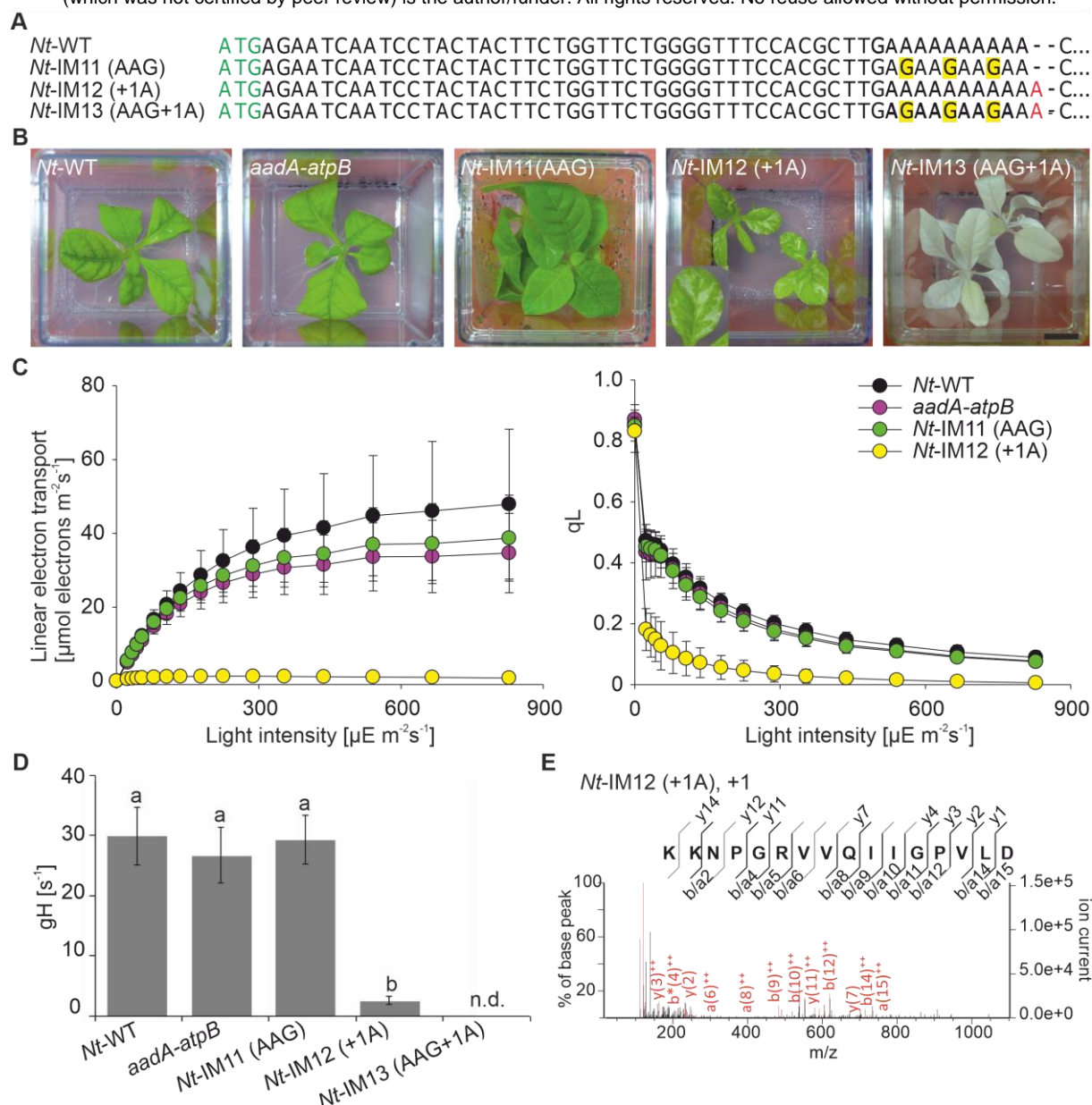
Figure 5. Generation and characterization of transplastomic tobacco plants carrying the I-iota mutation and/or disrupting the upstream oligoA stretch. A. Mutants generated to analyze recoding in tobacco. The sequence of the 5' part of *atpB* from the start codon (green) to the oligoA stretch are presented. Red letters represent insertions. Adenines replaced by guanines are highlighted in yellow. **B.** Phenotypes of transplastomic tobacco lines grown in sterile culture on sucrose-containing medium. **C.** Light-response curves of linear electron flux (left panel) and chlorophyll-*a* fluorescence parameter qL (a measure for the redox state of the PSII acceptor side; right panel) in the wild type (*Nt*-Wt) and transplastomic tobacco lines. 10 wild type plants and 3-10 plants per transplastomic line were measured. For each construct, at least two independently generated transplastomic lines were analyzed. Error bars represent standard deviation. **D**. Activity of the ATP synthase. 10 wild type plants and 3-10 plants per

transplastomic line were measured. For each construct, at least two independent transplastomic lines were analyzed. Columns display average data and standard deviation. Columns bearing the same letter indicate samples that were not significantly different ($p < 0.05$) according to one-way ANOVA with Holm-Sidak post-hoc testing. n.d – not detected. **E.** Analysis of the targeted AtpB peptide by LC-MS/MS (cf. Figure 3D).
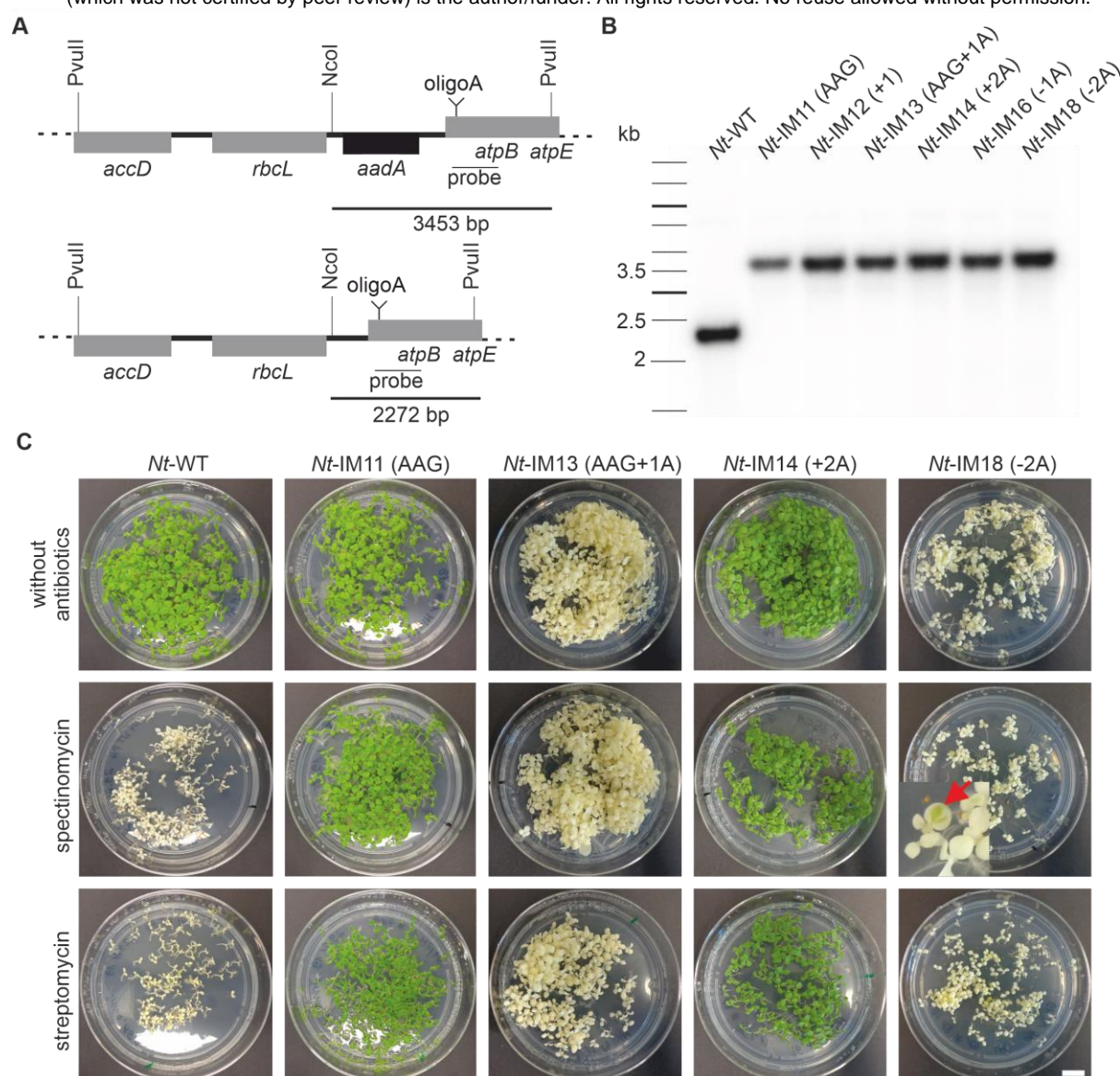
Figure 6. Confirmation of the homoplasmic state of transplastomic tobacco mutants.

A. Physical maps of the plastome region of transplastomic lines (top) and wild type (bottom) (modified after Rott et al., 2011). Tobacco genes are shown as grey boxes, the black box represents the *aadA* cassette. Restriction sites used for RFLP analysis are indicated. **B.** Restriction fragment length polymorphism analysis of transplastomic plants. DNA was digested with PvuII and NcoI. The location of the hybridization probe is indicated in **A**. The wild type (*Nt*-WT) shows the expected restriction fragment of 2.3 kb, while all transformants show only the transplastomic fragment of 3.5 kb, confirming their homoplasmic state. **C.** Inheritance test. Seeds were germinated on synthetic medium without antibiotic (control) or medium supplemented with either streptomycin or spectinomycin. *Nt*-IM11 (AAG) and *Nt*-IM14 (+2A) seeds were derived from homoplasmic plants, *Nt*-IM13 (AAG+1) and *Nt*-IM18 (-

2A) seeds were obtained from periclinal chimeras with mutated chloroplasts in their L2 layer (cf. Greiner, 2012) and Material and Methods). The red arrow indicates rare green spots on *Nt-IM18* (-2A) mutant leaves. Scale bar: 1cm.
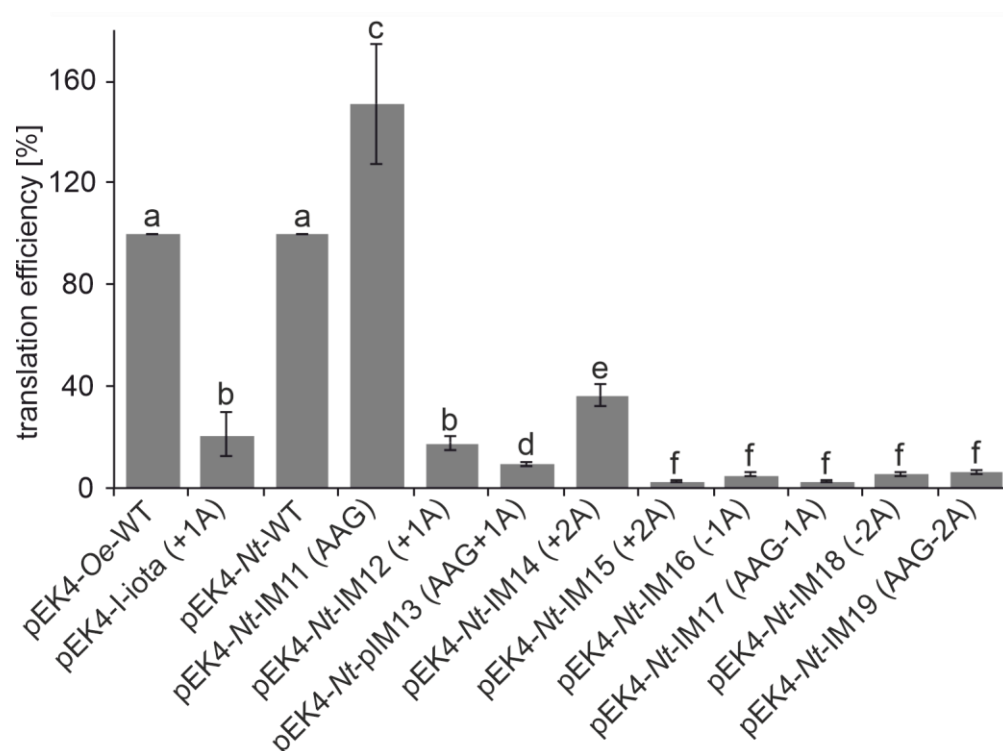
Figure 7. Impact of frameshift mutations in the oligoA stretch on translation efficiency as measured with the dual-luciferase system in *E. coli*. The error bars represent standard deviation from at least 3 independent biological replicates (i.e., bacterial colonies). Columns bearing the same letter indicate samples that were not significantly different ($p < 0.05$) according to one-way ANOVA with the Holm-Sidak post-hoc testing.
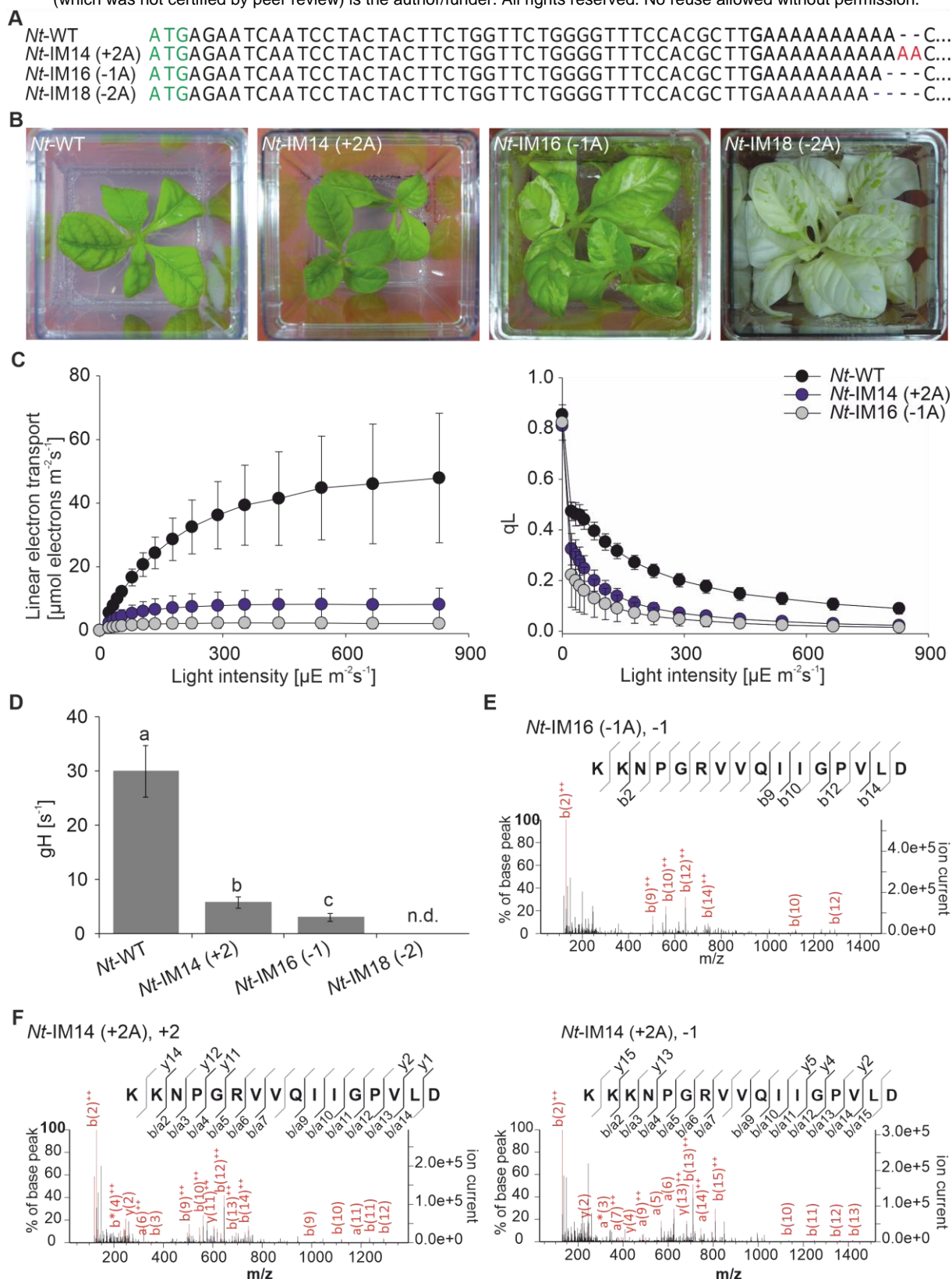
Figure 8. Generation and characterization of transplastomic tobacco mutants varying in the length of the oligoA stretch in *atpB*. A. Mutants generated to analyze recoding in tobacco. Red letters represent insertions, blue dashes denote deletions. **B**. Phenotypes of transplastomic

tobacco lines grown in sterile culture. **C.** Light-response curves of linear electron flux (left panel) and the chlorophyll *a* fluorescence parameter qL (a measure for the redox state of the PSII acceptor side; right panel) in the wild type (*Nt*-Wt) and transplastomic tobacco lines. 10 wild type plants and 3-10 plants per transplastomic line were measured. For each construct, at least two independently generated transplastomic lines were analyzed. Error bars represent standard deviation. **D.** ATP synthase activity. 10 wild type plants and 3-10 plants per transplastomic line were measured. For each construct, at least two independent transplastomic lines were analyzed. Columns display average data and standard deviation. Columns bearing the same letter indicate samples that were not significantly different ($p < 0.05$) according to one-way ANOVA with the Holm-Sidak post-hoc testing. **E,F**. Analysis of peptides derived from the slippery site in AtpB by LC-MS/MS (for detail see Figure 3D).
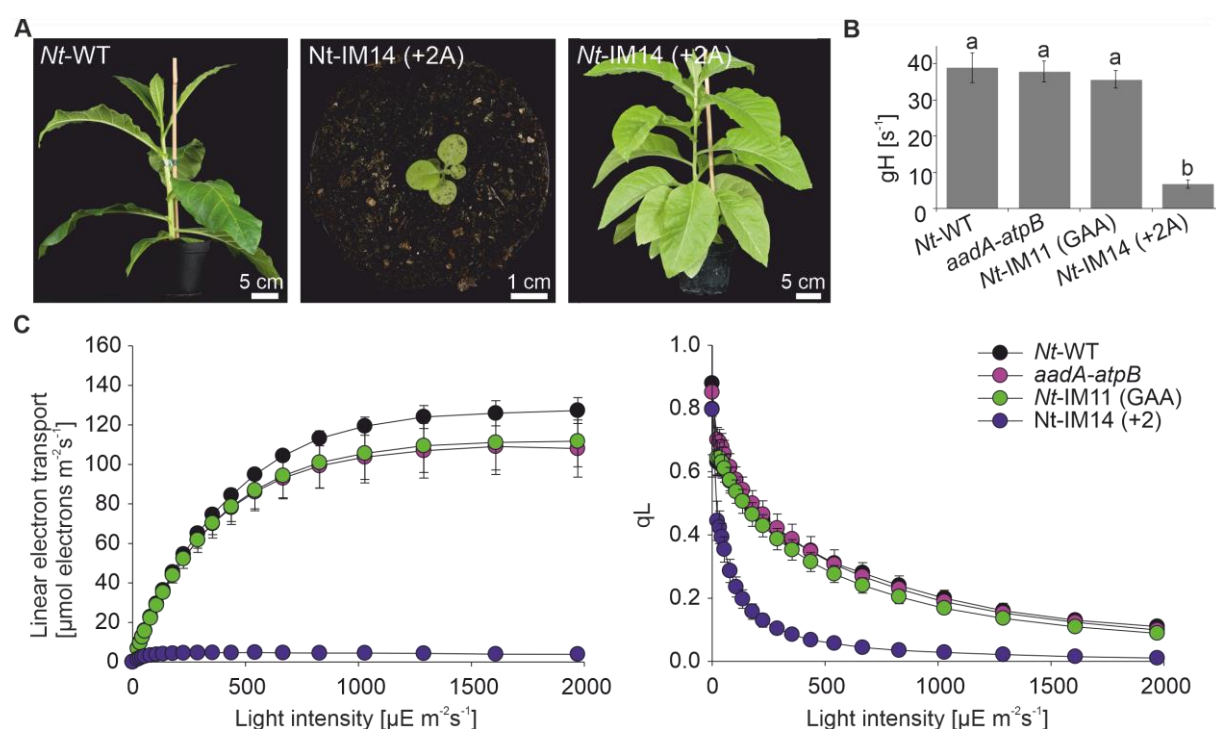
Figure 9. Correction of a +2 insertion in the *atpB* gene by recoding enables photoautotrophic growth. A. Growth phenotypes of wild type (*Nt*-Wt) and *Nt*-IM14 (+2A) plants cultivated in the greenhouse. Pictures were taken 7 weeks (left and middle) and 3 months (right photo) after germination. Note the strong retardation in growth of *Nt*-IM14 (+2A) mutants compared to the wild type. **B**. ATP synthase activity. *Nt*-WT, *aadA-atpB*, and *Nt*-IM11 (AAG) plants were 7 weeks old, *Nt*-IM14 (+2A) plants were 14 weeks old. 3 wild type plants and 3-5 plants per transplastomic line were measured. For each construct, at least two independent transplastomic lines were analyzed. Columns display average data and standard deviation. Columns bearing the same letter indicate samples that were not significantly different ($p < 0.05$) according to one-way ANOVA with Holm-Sidak post-hoc testing. **C**. Light-response curves of linear electron flux (left panel) and the chlorophyll *a* fluorescence parameter qL (a measure for the redox state of the PSII acceptor side; right panel) in the wild type and transplastomic tobacco lines. 4 wild type plants and 3-5 plants per transplastomic line were measured. For each construct, at least two independently generated transplastomic lines were analyzed. Error bars represent standard deviation.
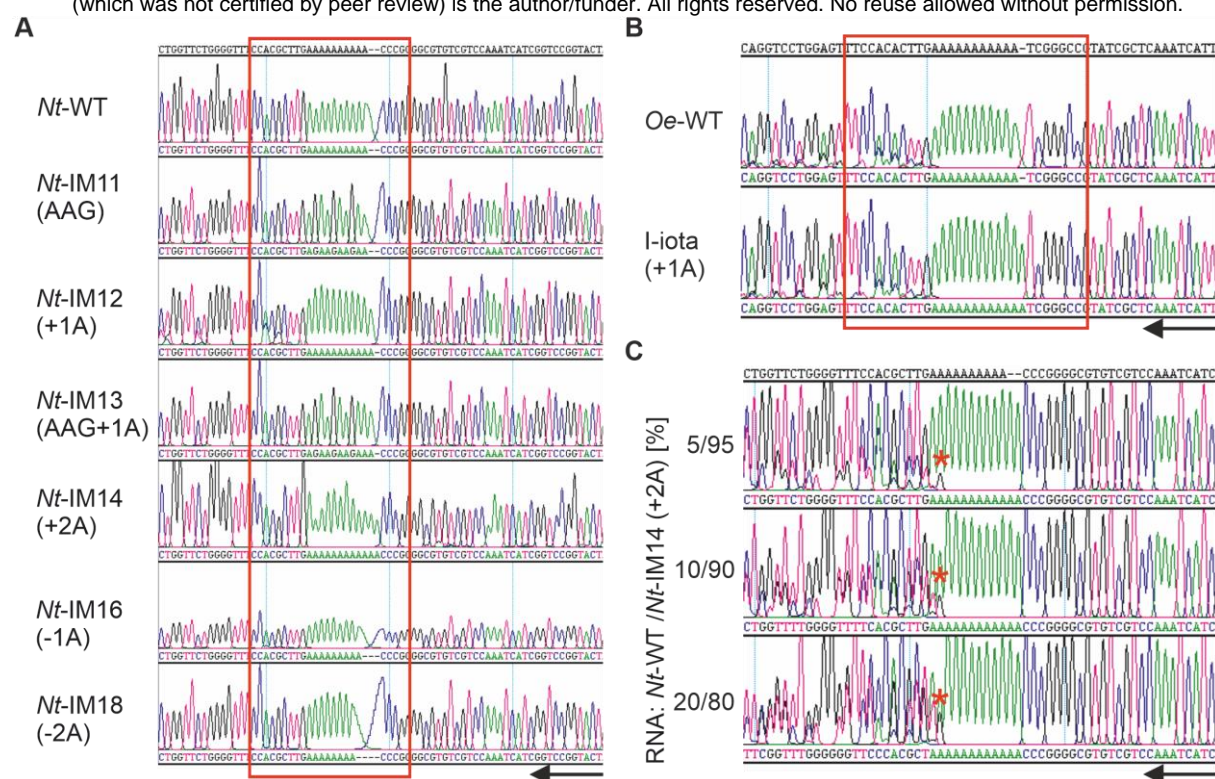
Figure 10. cDNA analysis to test for RNA polymerase stuttering in *atpB*. A. cDNA analysis of transplastomic tobacco plants and the wild type. The amplified cDNA population was sequenced, and typical Sanger sequencing chromatograms are presented. The sequence containing ther oligoA stretch is boxed in red. **B.** cDNA analysis of *Oenothera* wild type [*Oe*-WT) and I-iota (+1) plants. **C.** Sensitivity test for the detection of RNA polymerase stuttering. RNA was extracted from the wild type (*Nt*-WT) and the *Nt*-IM14 (+2A) transplastomic line, and the RNA samples were mixed in different ratios (indicated in %). cDNA was the synthesized, amplified and sequenced. Red asterisks indicate the additional peak, corresponding to the spiked-in wild-type RNA. Black arrows indicate the direction of the sequencing reaction.

Parsed Citations

Anikin M, Molodtsov V, Temiakov D, McAllister WT (2010) Transcript slippage and recoding. In JF Atkins, RF Gesteland, eds, Recoding: expansion of decoding rules enriches gene expression. Springer New York, New York, NY, pp 409-432
Google Scholar: Author Only Title Only Author and Title

Arezi B, Hogrefe HH (2007) Escherichia coli DNA polymerase III epsilon subunit increases Moloney murine leukemia virus reverse transcriptase fidelity and accuracy of RT-PCR procedures. Anal Biochem 360: 84-91
Google Scholar: Author Only Title Only Author and Title

Atkins JF, Loughran G, Bhatt PR, Firth AE, Baranov PV (2016) Ribosomal frameshifting and transcriptional slippage: From genetic steganography and cryptography to adventitious use. Nucleic Acids Res 44: 7007-7078
Google Scholar: Author Only Title Only Author and Title

Baranov PV, Atkins JF, Yordanova MM (2015) Augmented genetic decoding: global, local and temporal alterations of decoding processes and codon meaning. Nat Rev Genet 16: 517-529
Google Scholar: Author Only Title Only Author and Title

Baranov PV, Fayet O, Hendrix RW, Atkins JF (2006) Recoding in bacteriophages and bacterial IS elements. Trends Genet 22: 174-181
Google Scholar: Author Only Title Only Author and Title

Baranov PV, Hammer AW, Zhou J, Gesteland RF, Atkins JF (2005) Transcriptional slippage in bacteria: distribution in sequenced genomes and utilization in IS element gene expression. Genome Biol 6: R25
Google Scholar: Author Only Title Only Author and Title

Baranov PV, Wills NM, Barriscale KA, Firth AE, Jud MC, Letsou A, Manning G, Atkins JF (2011) Programmed ribosomal frameshifting in the expression of the regulator of intestinal stem cell proliferation, adenomatous polyposis coli (APC). RNA Biol 8: 637-647
Google Scholar: Author Only Title Only Author and Title

Barkan A (2011) Expression of plastid genes: organelle-specific elaborations on a prokaryotic scaffold. Plant Physiol 155: 1520-1532
Google Scholar: Author Only Title Only Author and Title

Belew AT, Dinman JD (2015) Cell cycle control (and more) by programmed -1 ribosomal frameshifting: implications for disease and therapeutics. Cell Cycle 14: 172-178
Google Scholar: Author Only Title Only Author and Title

Bock R (2001) Transgenic plastids in basic research and plant biotechnology. J Mol Biol 312: 425-438
Google Scholar: Author Only Title Only Author and Title

Bock R (2007) Structure, function, and inheritance of plastid genomes. In R Bock, ed, Cell and Molecular Biology of Plastids. Springer, Berlin, Heidelberg, New York, pp 29–63
Google Scholar: Author Only Title Only Author and Title

Bock R (2017) Witnessing genome evolution: experimental reconstruction of endosymbiotic and horizontal gene transfer. Annu Rev Genet 51: 1-22
Google Scholar: Author Only Title Only Author and Title

Bock R, Timmis JN (2008) Reconstructing evolution: gene transfer from plastids to the nucleus. Bioessays 30: 556-566
Google Scholar: Author Only Title Only Author and Title

Brierley I, Jenner AJ, Inglis SC (1992) Mutational analysis of the "slippery-sequence" component of a coronavirus ribosomal frameshifting signal. J Mol Biol 227: 463-479
Google Scholar: Author Only Title Only Author and Title

Caliskan N, Peske F, Rodnina MV (2015) Changed in translation: mRNA recoding by -1 programmed ribosomal frameshifting. Trends Biochem Sci 40: 265-274
Google Scholar: Author Only Title Only Author and Title

Caliskan N, Wohlgemuth I, Korniy N, Pearson M, Peske F, Rodnina MV (2017) Conditional switch between frameshifting regimes upon translation of dnaX mRNA. Mol Cell 66: 558-567.e554
Google Scholar: Author Only Title Only Author and Title

Doyle JJ (1990) Isolation of plant DNA from fresh tissue. Focus 12: 13-15
Google Scholar: Author Only Title Only Author and Title

Gesteland RF, Weiss RB, Atkins JF (1992) Recoding: reprogrammed genetic decoding. Science 257: 1640-1641
Google Scholar: Author Only Title Only Author and Title

Greiner S (2012) Plastome mutants of higher plants. In R Bock, V Knoop, eds, Genomics of chloroplasts and mitochondria. Springer, Dordrecht, Heidelberg, New York, London, pp 237–266
Google Scholar: Author Only Title Only Author and Title

Greiner S, Köhl K (2014) Growing evening primroses (Oenothera). Front Plant Sci 5: 38

Google Scholar: Author Only Title Only Author and Title

Greiner S, Wang X, Rauwolf U, Silber MV, Mayer K, Meurer J, Haberer G, Herrmann RG (2008) The complete nucleotide sequences of the five genetically distinct plastid genomes of Oenothera, subsection Oenothera: I. sequence evaluation and plastome evolution. Nucleic Acids Res 36: 2366-2378

Google Scholar: Author Only Title Only Author and Title

Grentzmann G, Ingram JA, Kelly PJ, Gesteland RF, Atkins JF (1998) A dual-luciferase reporter system for studying recoding signals. RNA 4: 479-486

Google Scholar: Author Only Title Only Author and Title

Hager M (2002) Anwendung reverser Genetic zur Fukntionsanalyse plastidenkodierter Gene. Inaugural-Dissertation. Albert-Ludwigs-Universität Freiburg i. Br.

Google Scholar: Author Only Title Only Author and Title

Hahn A, Vonck J, Mills DJ, Meier T, Kuhlbrandt W (2018) Structure, mechanism, and regulation of the chloroplast ATP synthase. Science 360

Google Scholar: Author Only Title Only Author and Title

Hausmann S, Garcin D, Delenda C, Kolakofsky D (1999) The versatility of paramyxovirus RNA polymerase stuttering. J Virol 73: 5568-5576

Google Scholar: Author Only Title Only Author and Title

Herrmann RG (1997) Eukaryotism, towards a new interpretation. In. Springer Berlin Heidelberg, Berlin, Heidelberg, pp 73-118

Google Scholar: Author Only Title Only Author and Title

Herrmann RG, Seyer P, Schedel R, Gordon K, Bisanz C, Winter P, Hildebrandt JW, Wlaschek M, Alt J, Driesel AJ, Sears BB (1980) The plastid chromosomes of several dicotyledons. In T Bücher, W Sebald, H Weiss, eds, Biological Chemistry of Organelle Formation. Springer Berlin Heidelberg, Berlin, Heidelberg, pp 97-112

Google Scholar: Author Only Title Only Author and Title

Ivanov IP, Gesteland RF, Atkins JF (2000) Antizyme expression: a subversion of triplet decoding, which is remarkably conserved by evolution, is a sensor for an autoregulatory circuit. Nucleic Acids Res 28: 3185-3196

Google Scholar: Author Only Title Only Author and Title

Ivanova NN, Schwientek P, Tripp HJ, Rinke C, Pati A, Huntemann M, Visel A, Woyke T, Kyrpides NC, Rubin EM (2014) Stop codon reassignments in the wild. Science 344: 909-913

Google Scholar: Author Only Title Only Author and Title

Jacks T, Madhani HD, Masiarz FR, Varmus HE (1988) Signals for ribosomal frameshifting in the Rous sarcoma virus gag-pol region. Cell 55: 447-458

Google Scholar: Author Only Title Only Author and Title

Jacques JP, Hausmann S, Kolakofsky D (1994) Paramyxovirus mRNA editing leads to G deletions as well as insertions. EMBO J 13: 5496-5503

Google Scholar: Author Only Title Only Author and Title

Jarvis P, López-Juez E (2013) Biogenesis and homeostasis of chloroplasts and other plastids. Nat Rev Mol Cell Biol 14: 787-802

Google Scholar: Author Only Title Only Author and Title

Karcher D, Bock R (2002) The amino acid sequence of a plastid protein is developmentally regulated by RNA editing. J Biol Chem 277: 5570-5574

Google Scholar: Author Only Title Only Author and Title

Ketteler R (2012) On programmed ribosomal frameshifting: the alternative proteomes. Front Genet 3: 242

Google Scholar: Author Only Title Only Author and Title

Kirk JTO, Telney-Basset RAE (1978) The plastids their chemistry, structure, growth and inheritance. Elsevier, Amsterdam/New York/Oxford

Google Scholar: Author Only Title Only Author and Title

Kohl S, Bock R (2009) Transposition of a bacterial insertion sequence in chloroplasts. Plant J 58: 423-436

Google Scholar: Author Only Title Only Author and Title

Koutmou KS, Schuller AP, Brunelle JL, Radhakrishnan A, Djuranovic S, Green R (2015) Ribosomes slide on lysine-encoding homopolymeric A stretches. Elife 4

Google Scholar: Author Only Title Only Author and Title

Kramer DM, Johnson G, Kiirats O, Edwards GE (2004) New fluorescence parameters for the determination of QA redox state and excitation energy fluxes. Photosynth Res 79: 209

Google Scholar: Author Only Title Only Author and Title

Kramer EB, Farabaugh PJ (2007) The frequency of translational misreading errors in E. coli is largely determined by tRNA competition. RNA 13: 87-96

Google Scholar: Author Only Title Only Author and Title

Kurland CG (1992) Translational accuracy and the fitness of bacteria. Annu Rev Genet 26: 29-50
Google Scholar: Author Only Title Only Author and Title

Kutzelnigg H, Stubbe W (1974) Investigation on plastome mutants in Oenothera: 1. General considerations. Subcell. Biochem 3: 73-89
Google Scholar: Author Only Title Only Author and Title

Laemmli UK (1970) Cleavage of structural proteins during the assembly of the head of bacteriophage T4. Nature 227: 680-685
Google Scholar: Author Only Title Only Author and Title

Landau AM, Lokstein H, Scheller HV, Lainez V, Maldonado S, Prina AR (2009) A cytoplasmically inherited barley mutant is defective in photosystem I assembly due to a temperature-sensitive defect in ycf3 splicing. Plant Physiol 151: 1802-1811
Google Scholar: Author Only Title Only Author and Title

Larsen B, Wills NM, Nelson C, Atkins JF, Gesteland RF (2000) Nonlinearity in genetic decoding: homologous DNA replicase genes use alternatives of transcriptional slippage or translational frameshifting. Proc. Natl. Acad. Sci. USA 97: 1683-1688
Google Scholar: Author Only Title Only Author and Title

Li Y, Firth AE, Brierley I, Cai Y, Napthine S, Wang T, Yan X, Kuhn JH, Fang Y (2019) Programmed -2/-1 ribosomal frameshifting in simarteriviruses: an evolutionarily conserved mechanism. J Virol 93
Google Scholar: Author Only Title Only Author and Title

Lin C-P, Ko C-Y, Kuo C-I, Liu M-S, Schafleitner R, Chen L-FO (2015) Transcriptional slippage and RNA editing increase the diversity of transcripts in chloroplasts: insight from deep sequencing of Vigna radiata genome and transcriptome. PloS One 10: e0129396-e0129396
Google Scholar: Author Only Title Only Author and Title

Linton MF, Pierotti V, Young SG (1992) Reading-frame restoration with an apolipoprotein B gene frameshift mutation. Proc. Natl. Acad. Sci. USA 89: 11431-11435
Google Scholar: Author Only Title Only Author and Title

Massouh A, Schubert J, Yaneva-Roder L, Ulbricht-Jones ES, Zupok A, Johnson MT, Wright SI, Pellizzer T, Sobanski J, Bock R, Greiner S (2016) Spontaneous chloroplast mutants mostly occur by replication slippage and show a biased pattern in the plastome of Oenothera. Plant Cell 28: 911-929
Google Scholar: Author Only Title Only Author and Title

McCutcheon JP, McDonald BR, Moran NA (2009) Origin of an alternative genetic code in the extremely small and GC-rich genome of a bacterial symbiont. PLoS Genet 5: e1000565
Google Scholar: Author Only Title Only Author and Title

Meydan S, Klepacki D, Karthikeyan S, Margus T, Thomas P, Jones JE, Khan Y, Briggs J, Dinman JD, Vazquez-Laslop N, Mankin AS (2017) Programmed ribosomal frameshifting generates a copper transporter and a copper chaperone from the same gene. Mol Cell 65: 207-219
Google Scholar: Author Only Title Only Author and Title

Miller WA, Giedroc DP (2010) Ribosomal frameshifting in decoding plant viral RNAs. In GR Atkins J., ed, Recoding: expansion of decoding rules enriches gene expression, Vol Nucleic Acids and Molecular Biology. Springer, New York, NY
Google Scholar: Author Only Title Only Author and Title

Moreno JC, Martinez-Jaime S, Schwartzmann J, Karcher D, Tillich M, Graf A, Bock R (2018) Temporal proteomics of inducible RNAi lines of Clp protease subunits identifies putative protease substrates. Plant Physiol 176: 1485-1508
Google Scholar: Author Only Title Only Author and Title

Murashige T, Skoog F (1962) A revised medium for rapid growth and bio assays with tobacco tissue cultures. Physiol Plantarum 15: 473-497
Google Scholar: Author Only Title Only Author and Title

Namy O, Moran SJ, Stuart DI, Gilbert RJ, Brierley I (2006) A mechanical explanation of RNA pseudoknot function in programmed ribosomal frameshifting. Nature 441: 244-247
Google Scholar: Author Only Title Only Author and Title

Napthine S, Vidakovic M, Girnary R, Namy O, Brierley I (2003) Prokaryotic-style frameshifting in a plant translation system: conservation of an unusual single-tRNA slippage event. EMBO J 22: 3941-3950
Google Scholar: Author Only Title Only Author and Title

Nishimura K, Kato Y, Sakamoto W (2017) Essentials of proteolytic machineries in chloroplasts. Mol Plant 10: 4-19
Google Scholar: Author Only Title Only Author and Title

Nishio JN, Whitmarsh J (1993) Dissipation of the proton electrochemical potential in intact chloroplasts (II. The pH gradient monitored by cytochrome f reduction kinetics). Plant Physiol 101: 89-96
Google Scholar: Author Only Title Only Author and Title

Olspert A, Chung BY, Atkins JF, Carr JP, Firth AE (2015) Transcriptional slippage in the positive-sense RNA virus family Potyviridae. EMBO Rep 16: 995-1004

Google Scholar: Author Only Title Only Author and Title

Parker J (1989) Errors and alternatives in reading the universal genetic code. Microbiol Rev 53: 273-298
Google Scholar: Author Only Title Only Author and Title

Peled-Zehavi HD, A. (2007) Translation and translational regulation in chloroplasts. In R Bock, ed, Cell and Molecular Biology of Plastids. Springer-Verlag, Berlin, pp 249–281
Google Scholar: Author Only Title Only Author and Title

Polard P, Prere MF, Chandler M, Fayet O (1991) Programmed translational frameshifting and initiation at an AUU codon in gene expression of bacterial insertion sequence IS911. J Mol Biol 222: 465-477
Google Scholar: Author Only Title Only Author and Title

Porra R, Thompson W, Kriedermann P (1989) Determination of accurate extinction coefficient and simultaneous equations for essaying chlorophylls a and b extracted with four different solvents: verification of the concentration of chlorophyll standards by atomic absorption spectroscopy. Biochim Biophys Acta 975: 384–394
Google Scholar: Author Only Title Only Author and Title

Ratinier M, Boulant S, Combet C, Targett-Adams P, McLauchlan J, Lavergne JP (2008) Transcriptional slippage prompts recoding in alternate reading frames in the hepatitis C virus (HCV) core sequence from strain HCV-1. J Gen Virol 89: 1569-1578
Google Scholar: Author Only Title Only Author and Title

Roberts JD, Bebenek K, Kunkel TA (1988) The accuracy of reverse transcriptase from HIV-1. Science 242: 1171-1173
Google Scholar: Author Only Title Only Author and Title

Rolland N, Dorne AJ, Amoroso G, Sultemeyer DF, Joyard J, Rochaix JD (1997) Disruption of the plastid ycf10 open reading frame affects uptake of inorganic carbon in the chloroplast of Chlamydomonas. EMBO J 16: 6713-6726
Google Scholar: Author Only Title Only Author and Title

Rott M, Martins NF, Thiele W, Lein W, Bock R, Kramer DM, Schottler MA (2011) ATP synthase repression in tobacco restricts photosynthetic electron transport, CO2 assimilation, and plant growth by overacidification of the thylakoid lumen. Plant Cell 23: 304-321
Google Scholar: Author Only Title Only Author and Title

Schaffner C, Laasch H, Hagemann R (1995) Detection of point mutations in chloroplast genes of Antirrhinum majus L. I. Identification of a point mutation in the psaB gene of a photosystem I plastome mutant. Mol Gen Genet 249: 533-544
Google Scholar: Author Only Title Only Author and Title

Schmitz-Linneweber C, Kushnir S, Babiychuk E, Poltnigg P, Herrmann RG, Maier RM (2005) Pigment deficiency in nightshade/tobacco cybrids is caused by the failure to edit the plastid ATPase alpha-subunit mRNA. Plant Cell 17: 1815-1828
Google Scholar: Author Only Title Only Author and Title

Schöttler MA, Tóth SZ, Boulouis A, Kahlau S (2015) Photosynthetic complex stoichiometry dynamics in higher plants: biogenesis, function, and turnover of ATP synthase and the cytochrome b6f complex. J Exp Bot 66: 2373-2400
Google Scholar: Author Only Title Only Author and Title

Sears BB, Herrmann RG (1985) Plastome mutation affecting the chloroplast ATP synthase involves a post-transcriptional defect. Curr Genet 9: 521-528
Google Scholar: Author Only Title Only Author and Title

Sobanski J, Giavalisco P, Fischer A, Kreiner JM, Walther D, Schöttler MA, Pellizzer T, Golczyk H, Obata T, Bock R, Sears BB, Greiner S (2019) Chloroplast competition is controlled by lipid biosynthesis in evening primroses. Proc. Natl. Acad. Sci. USA 116: 5665-5674
Google Scholar: Author Only Title Only Author and Title

Stubbe W, Herrmann RG (1982) Selection and maintenance of plastome mutants and interspecific genome/plastome hybrids from Oenothera. In HR Edelman M, Chua N-H, ed, Methods in chloroplast molecular biology. Elsevier, Amsterdam/New York/Oxford, pp 149–165
Google Scholar: Author Only Title Only Author and Title

Su HJ, Barkman TJ, Hao W, Jones SS, Naumann J, Skippington E, Wafula EK, Hu JM, Palmer JD, dePamphilis CW (2019) Novel genetic code and record-setting AT-richness in the highly reduced plastid genome of the holoparasitic plant Balanophora. Proc. Natl. Acad. Sci. USA 116: 934-943
Google Scholar: Author Only Title Only Author and Title

Svab Z, Maliga P (1993) High-frequency plastid transformation in tobacco by selection for a chimeric aadA gene. Proc. Natl. Acad. Sci. USA 90: 913-917
Google Scholar: Author Only Title Only Author and Title

Tamas I, Wernegreen JJ, Nystedt B, Kauppinen SN, Darby AC, Gomez-Valero L, Lundin D, Poole AM, Andersson SG (2008) Endosymbiont gene functions impaired and rescued by polymerase infidelity at poly(A) tracts. Proc. Natl. Acad. Sci. USA 105: 14934-14939
Google Scholar: Author Only Title Only Author and Title

Thompson JD, Higgins DG, Gibson TJ (1994) CLUSTAL W: improving the sensitivity of progressive multiple sequence alignment through sequence weighting, position-specific gap penalties and weight matrix choice. Nucleic Acids Res 22: 4673-4680

Google Scholar: Author Only Title Only Author and Title

Timmis JN, Ayliffe MA, Huang CY, Martin W (2004) Endosymbiotic gene transfer: organelle genomes forge eukaryotic chromosomes. Nat Rev Genet 5: 123-135
Google Scholar: Author Only Title Only Author and Title

Tsiatsiani L, Heck AJ (2015) Proteomics beyond trypsin. FEBS J 282: 2612-2626
Google Scholar: Author Only Title Only Author and Title

van der Horst S, Snel B, Hanson J, Smeekens S (2019) Novel pipeline identifies new upstream ORFs and non-AUG initiating main ORFs with conserved amino acid sequences in the 5' leader of mRNAs in Arabidopsis thaliana. RNA 25: 292-304
Google Scholar: Author Only Title Only Author and Title

Vögele K, Schwartz E, Welz C, Schiltz E, Rak B (1991) High-level ribosomal frameshifting directs the synthesis of IS150 gene products. Nucleic Acids Res 19: 4377-4385
Google Scholar: Author Only Title Only Author and Title

Volchkov VE, Becker S, Volchkova VA, Ternovoj VA, Kotov AN, Netesov SV, Klenk HD (1995) GP mRNA of Ebola virus is edited by the Ebola virus polymerase and by T7 and vaccinia virus polymerases. Virology 214: 421-430
Google Scholar: Author Only Title Only Author and Title

Wernegreen JJ, Kauppinen SN, Degnan PH (2010) Slip into something more functional: selection maintains ancient frameshifts in homopolymeric sequences. Mol Biol Evol 27: 833-839
Google Scholar: Author Only Title Only Author and Title

Yamao F, Muto A, Kawauchi Y, Iwami M, Iwagami S, Azumi Y, Osawa S (1985) UGA is read as tryptophan in Mycoplasma capricolum. Proc. Natl. Acad. Sci. USA 82: 2306-2309
Google Scholar: Author Only Title Only Author and Title

Zoschke R, Bock R (2018) Chloroplast translation: structural and functional organization, operational control, and regulation. Plant Cell 30: 745-770
Google Scholar: Author Only Title Only Author and Title

Zoschke R, Kroeger T, Belcher S, Schöttler MA, Barkan A, Schmitz-Linneweber C (2012) The pentatricopeptide repeat-SMR protein ATP4 promotes translation of the chloroplast atpB/E mRNA. Plant J 72: 547-558
Google Scholar: Author Only Title Only Author and Title

Zuker M (2003) Mfold web server for nucleic acid folding and hybridization prediction. Nucleic Acids Res 31: 3406-3415
Google Scholar: Author Only Title Only Author and Title